CHAPTER 4

RESULTS AND DISCUSSIONS

4.1 Evidence of the formation of N-phthaloylchitosan

Phthaloylation of chitosan involved substitution of phthalic anhydride to the N atom of chitosan after the two hydrogens were removed. The proposed mechanism for the synthesis of phthaloylchitosan is shown in *Scheme 4.1*. Confirmation of the structural of phthaloylated chitosan was made using FTIR and ^{1}H NMR. Further characterization using XRD and solubility are also presented in this chapter.

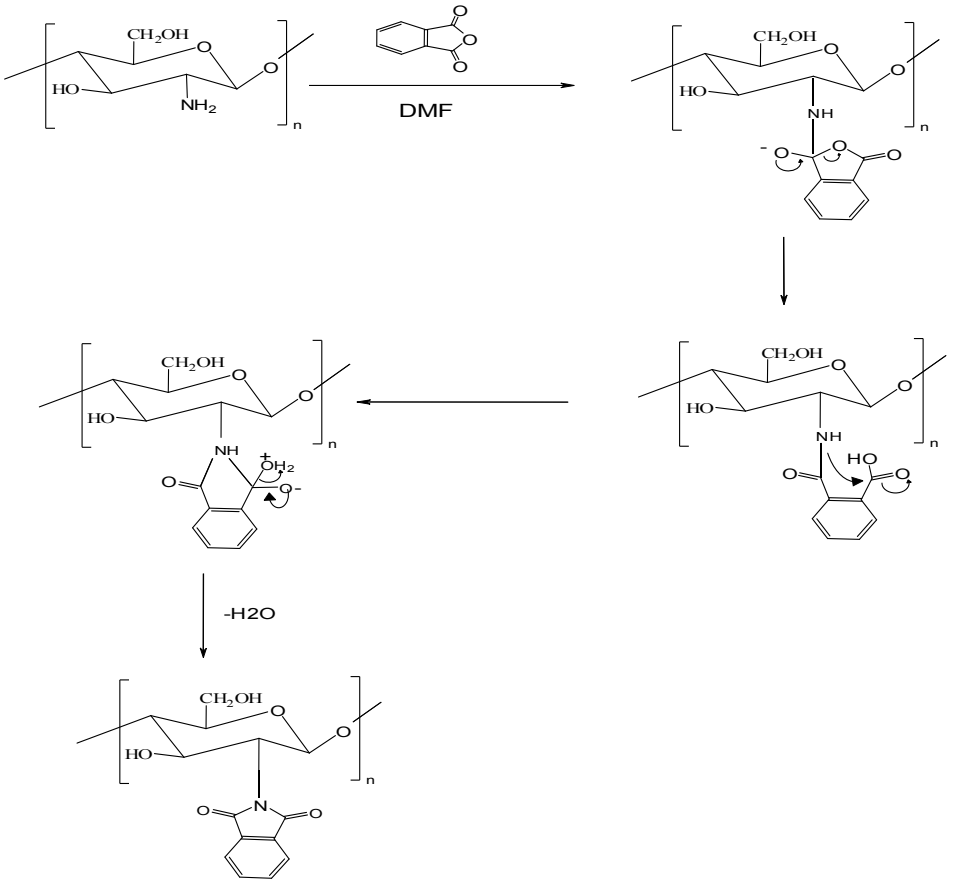

Scheme 4.1: Reaction of N-phthaloylation of chitosan [94]

4.1.1 FTIR

In FTIR spectra the position, intensity, and shape of characteristic absorption band are helpful in identifying functional groups, thus the chemical structure of the compound. The FTIR spectra of pure chitosan have been compared with the spectra of phthaloylated product, PhCh in *Figure 4.1*. The NH_2 band appearing around 1601 cm^{-1} in the pure chitosan spectra (*Figure 4.1(a)*) has disappeared indicating that substitution has occurred onto the N atom of chitosan. Spectrum of pure phthaloylchitosan (*Figure 4.1(b)*) exhibits peaks corresponding to the carbonyl amide at 1772 and 1708 cm^{-1}.There is also an absorption peak at 719 cm^{-1} indicating the presence of aromatic ring. These results verified the synthesis of N-phthaloylchitosan. Previous works have reported that three main peaks appeared after phthaloylation took place onto the amino group of chitosan [71,72,75,95]. Two of the peaks that belong to phthalimido group arise at 1711-1715 cm^{-1} and 1772-1777 cm^{-1}. The third band is dedicated to aromatic group which appeared at 721 cm^{-1} wavenumber. The details were presented in *Table 4.1*.

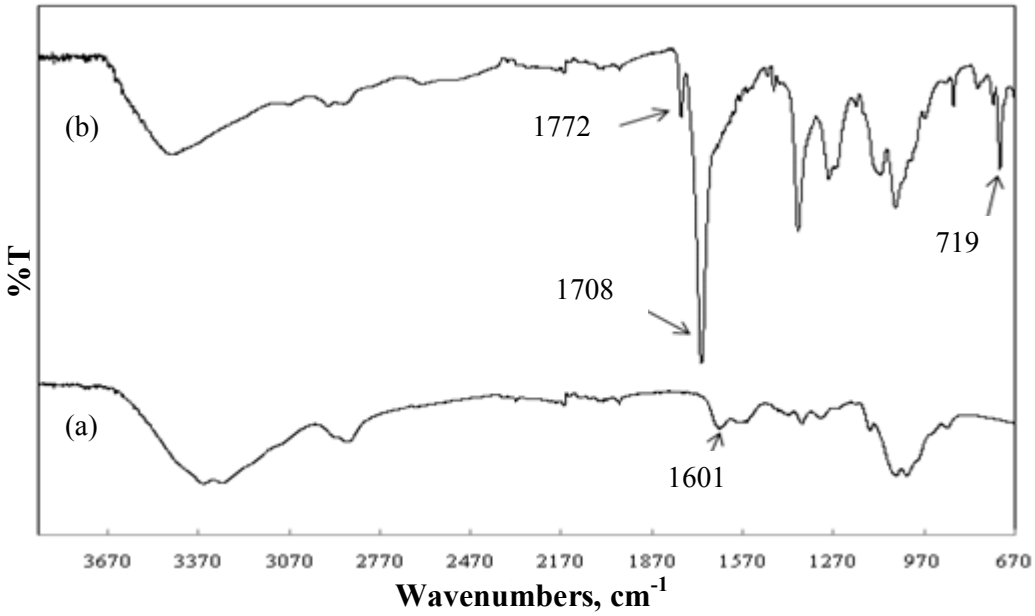

Figure 4.1: FTIR spectra of (a) chitosan, (b) phthaloylchitosan

Table 4.1: Significant wavenumbers exhibited by N-phthaloylated chitosan

Vibrational mode	Current study	Literature review	References
Phthalimido group	1772, 1708	1712, 1777	Liu et. al [95],
		1712, 1776	Kurita et. al [77-78],
			Bian et. al [72],
		1714, 1777	Rout et. al [71],
		1714, 1776	Yoksan et. al [75]
		1711, 1777	Janaciauskaite et. al [7]
		1710,1770	Nishimura et. al [96]
Aromatic group	719	721	Liu et. al [95],
			Bian et. al [72],
			Rout et. al [71],
			Yoksan et. al [75],
			Janaciauskaite et. al [7],
			Kurita et. al [77-78],

Treatment of chitosan with phthalic anhydride generally results in partial O-phthaloylation in addition to the N-subtitution [97] as shown in *Scheme 4.2*. From the FTIR spectra in *Figure 4.1(b)*, small extent of O-phthaloylation has also occurred in addition to N-phthaloylation as the peaks at 1240-1300 cm^{-1} were observed. Previous work by Kurita et. al [98], showed the similar observation of O-Phthaloylation.

Sometimes, O-phthaloyl group is an obstacle in most cases for quantitative and regioselective substitution [98]. However, in this study, since we used PhCh as the end product, small extent O-phthaloylation will not be a problem. Chemoselective full N-phthaloylation is possible by using mixture of DMF and hydroxyl-bearing co-solvent as the medium for refluxing. Although O-phthaloylation occurs in the initial stage under these

conditions, the ester linkage would be eventually cleaved by the water formed in the N-phthaloylation process [70].

Co-solvents that have been studied by Kurita et. al [98] include ethanol, ethylene glycol, methyl cellosolve and water in order to control the N-phthaloylation. Of the four co-solvents examined, water proved to be the most appropriate, whereby the product was much lighter in color and furthermore, the degree of substitution of the product was confirmed to be 1.0.

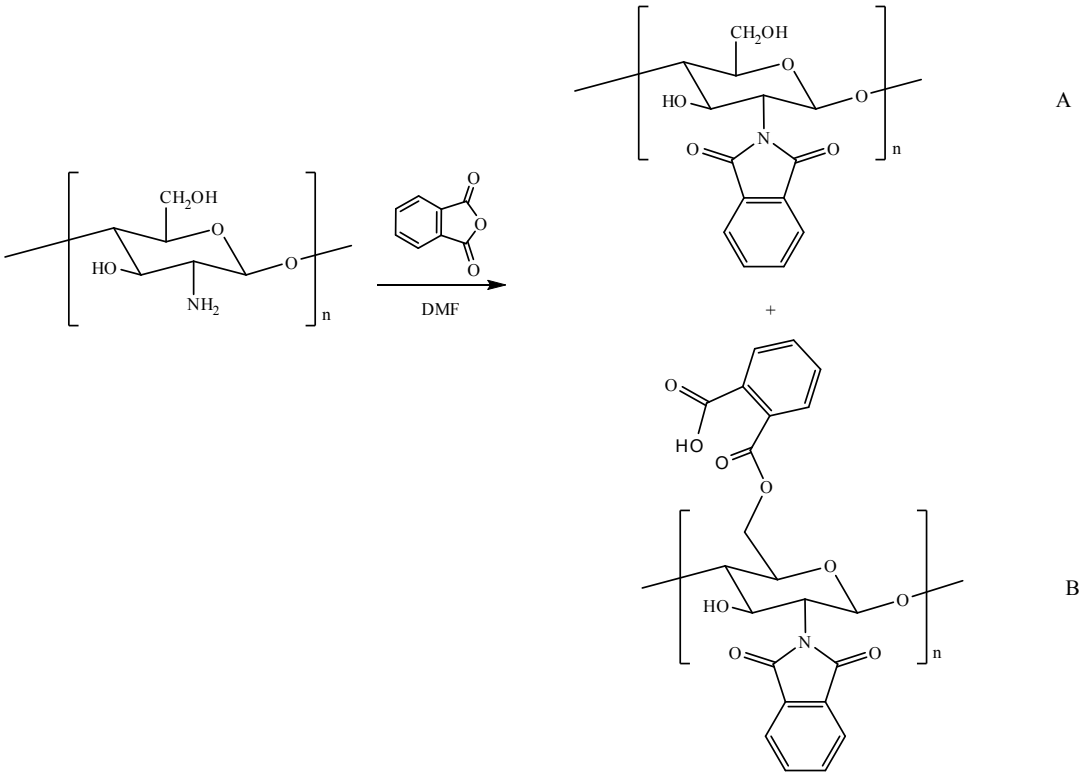

Scheme 4.2: Structure of A) N-phthaloylated chitosan and B) N,O-phthaloylated chitosan.

4.1.2 ^{1}H NMR

Confirmation of the structure of the synthesized PhCh via ^{1}H NMR is presented in *Figure 4.2*. ^{1}H NMR spectrum exhibits two distinct sets of signals. One set consists of peaks centering at 7.5, 7.7 and 7.9 ppm assigned to phthaloyl group. The signal peaks for the aromatic ring protons in PhCh occur in the 7.0 to 8.0 ppm region as other kinds of protons usually do not resonate in this region. Yoksan et. al [75] also observed peak at 7.6 ppm belonging to protons of the phenyl rings for successful phthaloylation. Peaks that exist between 2.0 and 5.0 ppm are dedicated to the chitosan backbone hydrogen atoms. Small extent of O-phthaloylation has also occurred in addition to N-phthaloylation as peaks attributed to O-phthaloyl group appear at 7.3-7.5 ppm [70,73]. This is supported by the FTIR results where bands at region 1240 - 1300 cm^{-1} due to the O-phthalimido group were observed [98]. FTIR and ^{1}H NMR results imply that phthaloylation has occurred onto chitosan to produce N-phthaloylchitosan and to a lesser extent N,O-phthaloylchitosan.

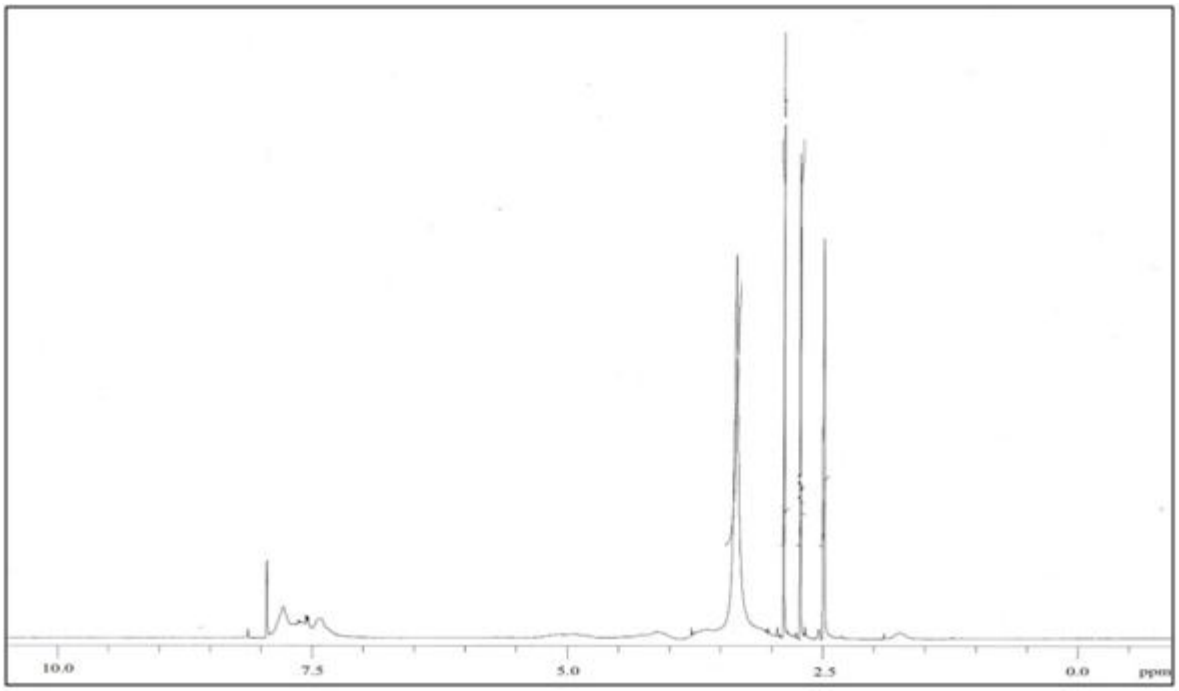

Figure 4.2: ^{1}H NMR spectra of phthaloylated chitosan

4.1.3 Physical properties of N-PhCh

4.1.3.1. Crystallinity

Comparison of XRD patterns for chitosan and modified chitosan can be observed in *Figure 4.3*. Chitosan exhibits two clear peaks at 2θ = 15.1° and 20.6°. After chitosan has been phthaloylated, the peaks merged to a one broad peak at 2θ = 21.7°. This shows that the nature of phthaloylchitosan is less crystalline compared to the chitosan. Observation can be made from *Scheme 4.3* that the bulkiness of the phthalimido groups results in the reduction of inter- and intramoleculear hydrogen bonds of the chitosan [75], thus disrupting its crystallinity.

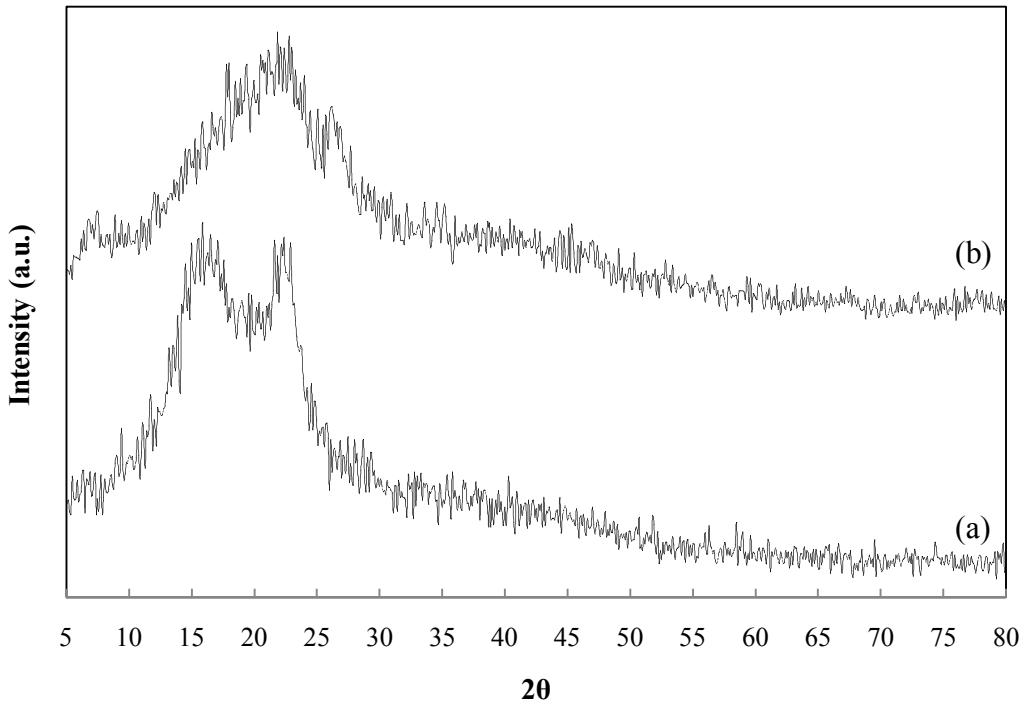

Figure 4.3: XRD pattern for (a) chitosan and (b) phthaloylated chitosan

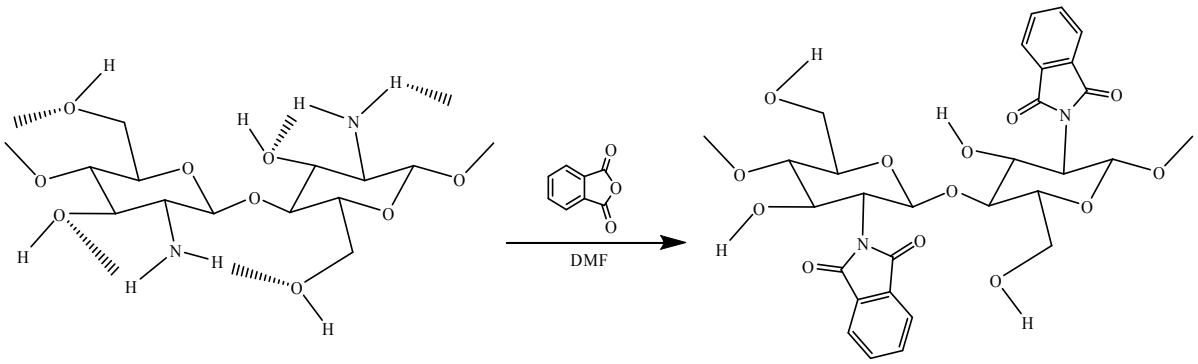

Scheme 4.3: Disruption of hydrogen bonds after phthaloylation

In addition, the heterogeneous structure of PhCh owing to the partial O-substitution also contributes to the amorphous nature [98]. Kurita et. al [98] had prepared N-phthaloylchitosan (without O-substitution) in DMF/water and obtained certain crystallinity as shown in *Figure 4.4*. Thus, PhCh with addition of O-phthaloylation is preferable as it fulfill the criteria of an electrolyte. Polymer electrolyte has to be in an amorphous state as crystallinity prevents mobile species from migrating under AC signal due to the rigid polymer chains [96].

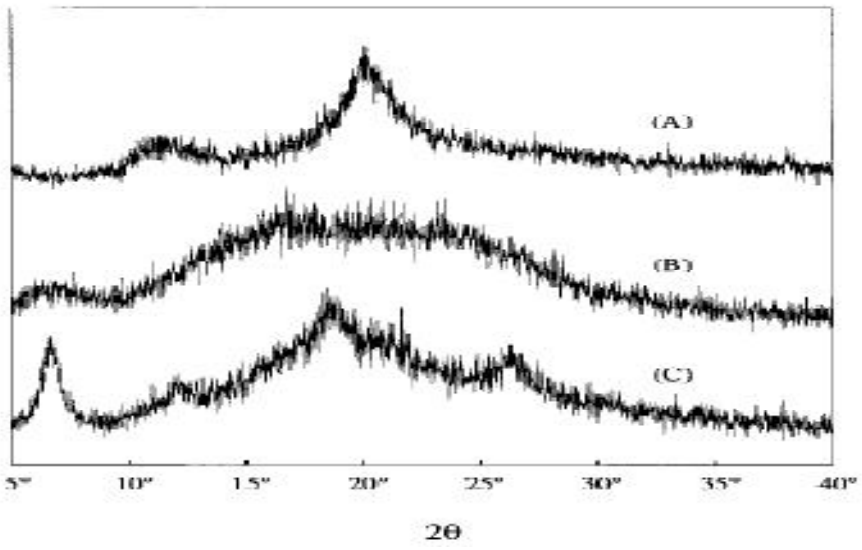

Figure 4.4: X-ray diffraction diagrams of (A) fully deacetylated chitosan, (B) phthaloyl-chitosan (ds 1.54) prepared in DMF, and (C)N-phthaloylchitosan (ds 1.00) prepared in DMF/water (95/5) [98]

4.1.3.2. Solubility

An amorphous polymer contains a network of entangled, flexible chains in a continuous motion. In the presence of solvent, the polymer network will swell from the osmotic activity of the solvent and the segmental motion will finally increase. The polymer will continue to expand with excess of solvent and increase its freedom to move sufficiently to allow transitional movement to the chains thereafter the substances will separate out to form a solution. Further dilution will result in the intermolecular forces that exist between the polymers chains will become less and finally the solution properties will only exhibit polymer-solvent interaction forces.

In this work, solubility test was done in order to compare the solubility of the product after chitosan has been phthaloylated. Three classes of solvents were identified;

I. *Polar aprotic solvents*: An aprotic polar solvent is not a hydrogen bond donor because it does not have hydrogen attached to oxygen or to nitrogen, so there are no positively charged hydrogens to form ion-dipole interactions [59].
II. *Polar protic solvents*: Protic solvents are hydrogen bond donor. The solvents molecules arrange themselves so that their partially positively charged hydrogens points toward the negatively charged species [59].
III. *Non-polar solvents*. Non-polar solvent has low dielectric constant and are poor insulator.

Table 4.2 shows the solubility of PhCh in various solvents. The results show that phthaloylated chitosan is soluble in most polar aprotic solvents. Complete dissolution was

observed in DMF, DMSO, DMAc and pyridine giving clear solutions compared to pure chitosan.

Table 4.2: Solubility of PhCh in various solvents

Solvents	Chitosan	PhCh
Polar solvents		
DMF	-	√
THF	-	-
DMAc	-	√
Pyridine	-	√
DMSO	-	√
Acetone	-	-
Ethyl Acetate	-	-
Acetic acid	√	-
Methanol	-	-
Cyclohexanone	-	-
Acetonitrile	-	-
Non-polar solvents		
Chloroform	-	-
Hexane	-	-
Toluene	-	-

√: soluble -: insoluble

N,O-phthaloylchitosan was shown to be more soluble in organic solvents compared to N-phthaloylchitosan as it swells in DMF and pyridine [70]. The N-substituted derivative was soluble in some solvents such as dichloroacetic acid, m-cresol, N,N-dimethylacetamide/LiCl and methanol/$CaCl_2$•$2H_2O$ while N,O-substituted derivative showed much higher solubility because of the bulky structure and amorphous nature in contrast to the crystalline structure of N-phthaloyled chitosan [98].

Clearly, acetamido or primary amino groups of chitosan have an important role in the formation of peculiar conformational features through intra/inter molecular hydrogen bonding. Therefore, removal of the two hydrogen atoms of amino groups of chitosan and introduction of some hydrophobic nature by chemical modifications will cause destruction of its inherent crystalline structure, resulting in the improvement of solubility in general organic solvents [99]. Evidence of the phthaloyl group being attached to the amino group is further shown due to it being insoluble in acetic acid, an acidic solvent. This solubility of phthaloylated chitosan may be partly attributable to the less crystallinity as confirmed by XRD results in *Section 4.1.3.1* [98].

The general rule that explains solubility on the basis of the polarity of molecules is that "like dissolves like" [59]. In other words, polar compounds dissolve in polar solvents and non-polar compounds dissolve in non-polar solvents. Polar solvents have high dielectric constant which is a measure of how well the solvent can insulate opposite charges from one another. Polar solvent has partial charges that can interact with the partial charges on a polar compound. The negative poles of the solvent molecules surround the positive poles of the polar solute and vice versa. For a specific polymer, its solubility in a solvent can be predicted from the solubility parameter.

Table 4.3: Density of PhCh

Test	Mass/ g	Volume/ mL	Density/ ρ	δ_{pol}
1	0.5005	0.34	1.47	24.37
2	0.5070	0.33	1.54	25.53
3	0.5054	0.35	1.44	23.87

$$Average\ \delta_{pol} = 24.59$$

$$\approx 24.6$$

The greatest tendency of a polymer to dissolve occurs when its solubility parameter matches that of the solvents, meaning that the difference between solubility parameter of solvent and polymer, $\Delta\delta = \left| \delta_{pol} - \delta_{sol} \right|$ is small. By using density of PhCh shown in *Table 4.3,* average of δ_{pol} obtained is 24.6. From *Table 4.2*, we can see that PhCh soluble in mostly polar aprotic solvents compared to protic and non-polar solvents. Polar aprotic solvents are good solvents as PhCh dissolved completely in DMF, DMSO, DMAc and pyridine. The four solvents show small $\Delta\delta$ in a range of 0.3 to 2.8. However, DMF exhibits the best solvent as the solubility parameter closely matches that of the polymer with smallest $\Delta\delta$ value of 0.3. The $\Delta\delta$ values of polar protic solvents shown in *Table 4.4*, it is agreeable with the solubility results of PhCh. The value of solubility parameter of the solvents and polymer is not match with the difference are in the range of 3.2 to 7.8 and this reflects the poor solubility of PhCh in these solvents. The same result is also obtained by non-polar solvents which show the largest value of $\Delta\delta$ from 5.7 to 9.7, with hexane exhibited the worst solvent for PhCh. Thus, the results listed in *Table 4.4* indicate that the difference between calculated (estimation by solubility parameters) and experimentally results are in consensus. In view of this, with the lowest differential value between δ_{sol} and δ_{pol} was chosen in order to get homogeneous solution to prepare PhCh based polymer electrolytes.

Table 4.4: Hansen solubility parameter of solvents

Solvents	δ_D	δ_P	δ_H	δ_{sol}	$\Delta\delta$
		Polar aprotic solvent			
DMF	**17.4**	**13.7**	**11.3**	**24.9**	***0.3***
THF	16.8	5.7	8.0	19.5	*5.1*
DMAc	**16.8**	**11.5**	**10.2**	**22.8**	***1.8***
Pyridine	**19.0**	**8.8**	**5.9**	**21.8**	***2.8***
DMSO	**18.4**	**16.4**	**10.2**	**26.7**	***2.1***
Acetone	15.5	10.4	7.0	19.9	*4.7*
Ethyl Acetate	15.8	5.3	7.2	18.2	*6.4*
Acetonitrile	15.3	18.0	6.1	24.4	*0.2*
		Polar protic solvents			
Methanol	15.1	12.3	22.3	29.6	*5.0*
Cyclohexanone	16.8	0	0.2	16.8	*7.8*
Acetic acid	14.5	8	13.5	21.4	*3.2*
		Non-polar solvents			
Chloroform	17.8	3.1	5.7	18.9	*5.7*
Hexane	14.9	0	0	14.9	*9.7*
Toluene	18.0	1.4	2.0	18.2	*6.4*

$\delta_{pol} = 24.6$

4.2 Phthaloylchitosan-based Polymer Electrolytes

4.2.1. PhCh Film forming

Phthaloylated chitosan was used for the first time as a polymer electrolyte host instead of it being usually used as an intermediate in the synthesizing process [74-76]. In this study, PhCh as solid polymer electrolyte doped with lithium iodide, in the film form were characterized by FTIR spectroscopy, XRD and also EIS.

Following the results from solubility in *Section 4.1.3.2*, with solubility parameter of 24.9 closely matches that of PhCh with the solubility parameter of 24.2, DMF was chosen as the solvent in the polymer electrolyte film forming. Compatibility of the polymer with the solvents is important in order to obtain homogeneous solution for film casting. The films containing LiI were all transparent. The yellowish color of pure PhCh film is observed to become darker with increasing of LiI concentration as shown in the *Figure 4.5* due to the oxidation of iodide to iodine. PhCh-LiI polymer electrolyte system was introduced until 50 wt.% of salt. On addition of more than 50 wt.% LiI, a free standing film cannot be formed. Thus, in this work, preparation of polymer electrolyte was stopped until 50 wt.% of LiI.

Comparison of the FTIR spectra of PhCh in two different forms, powder and film, is shown in *Figure 4.6*. Although the spectrum for both powder and film forms are similar, PhCh spectra in film form is observed to have better transmission compared to powder. From the spectrum of PhCh in film form (*Figure 4.6(b)*), a small peak was observed at 1654 cm^{-1} assigned to amide group which is not found in PhCh in powder form. Assumption has been made if there is still DMF left in the film. However, not all the sharp bands belonging to DMF (*Figure 4.6(c)*) appear in the PhCh film spectrum, as band at 1087 cm^{-1} does not appear in the film spectrum. Thus, from these observations it suggested that transformation of the structure of PhCh might have occurred as shown in *Scheme 4.4*.

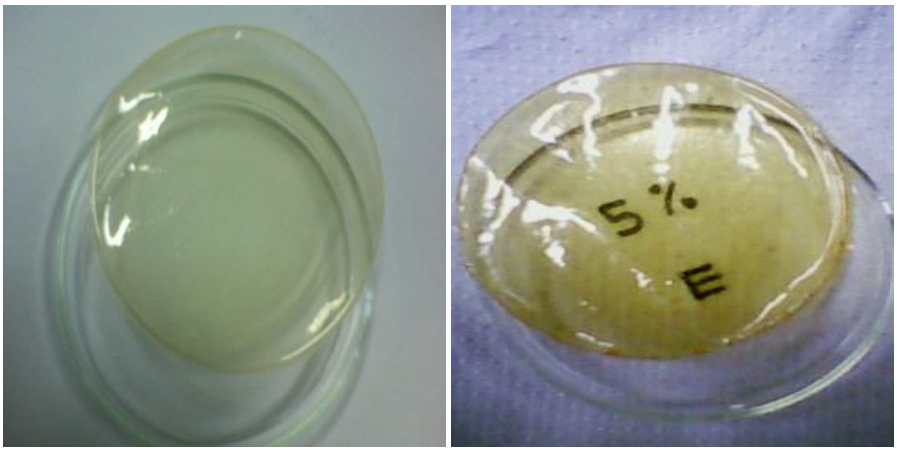

(a) (b)

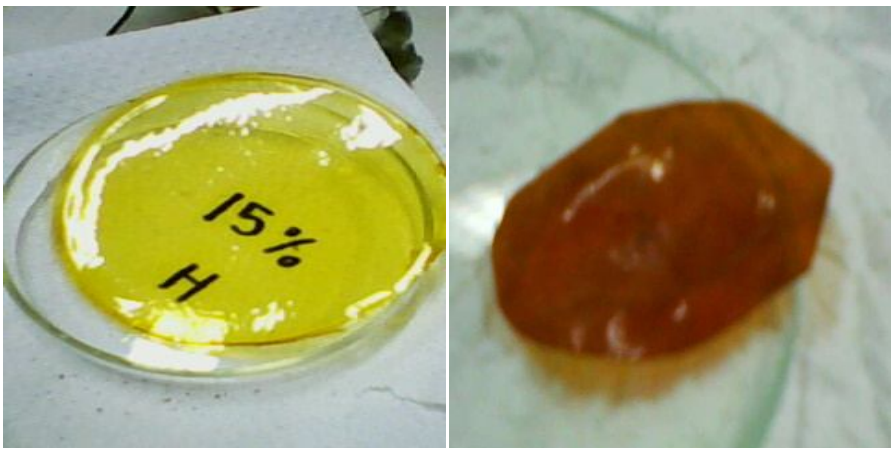

(c) (d)

Figure 4.5: Photograph of PhCh films; (a) pure (b) 5 wt.% LiI (c) 15 wt.% LiI and (d) 25 wt.% of LiI

The transformation is believed to occur in the presence of DMF which is a versatile dipolar aprotic solvent that greatly enhances the nucleophilicity of the anions, I^- in reactions. For instance, when heated with an acid chloride or anhydride, it furnishes the corresponding amide [100]. This statement is strongly supported by the arising of peak amide at 1654 cm^{-1} in the PhCh film spectrum. Detail of the results will be further discussed in *Section 4.2.2* after LiI is added to PhCh.

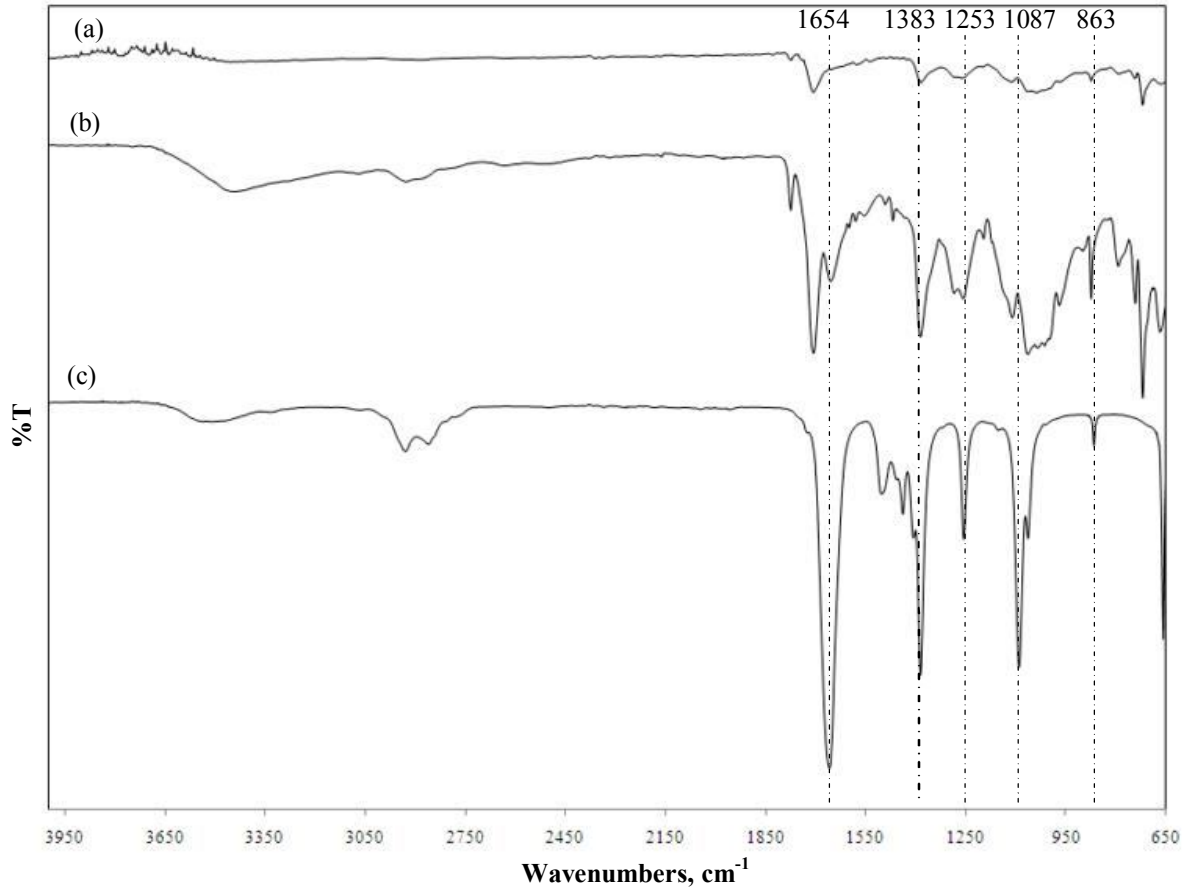

Figure 4.6: FTIR spectra of phthaloylchitosan in a (a) powder and (b) film form with (c) DMF

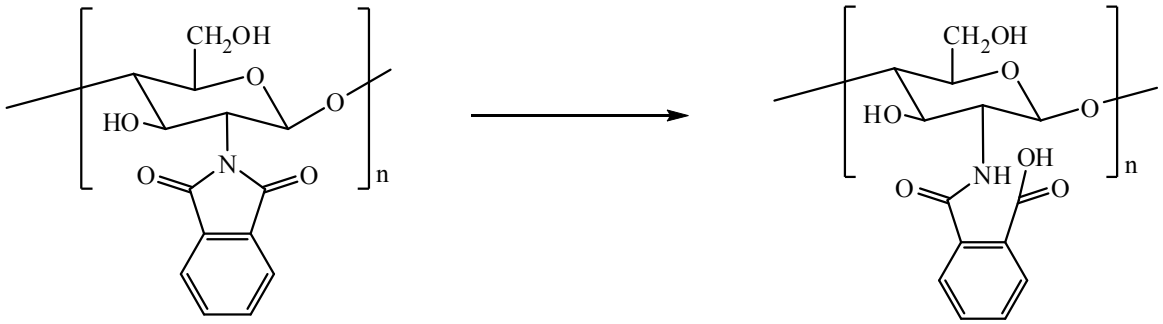

Scheme 4.4: Transformation of the phthaloylchitosan

4.2.2. Interaction between PhCh and lithium iodide

FTIR is an important method used to confirm the complexation between the salt and the polymer. Several researchers used this method to study the interaction between polymer, salt and also plasticizers [19]. Lithium iodide was doped in the PhCh based polymer electrolytes in various weight percentages from 5 to 50. The entire spectra from range 650 to 4000 cm^{-1} are shown in *Figure 4.7*. Several changes are spotted from the spectra as LiI content is increased. Some of the significant peaks changes can be observed in the phthalimido region, in the range of 1500 to 1800 cm^{-1} (*Figure 4.8*) and 700 to 750 cm^{-1} (*Figure 4.9*).

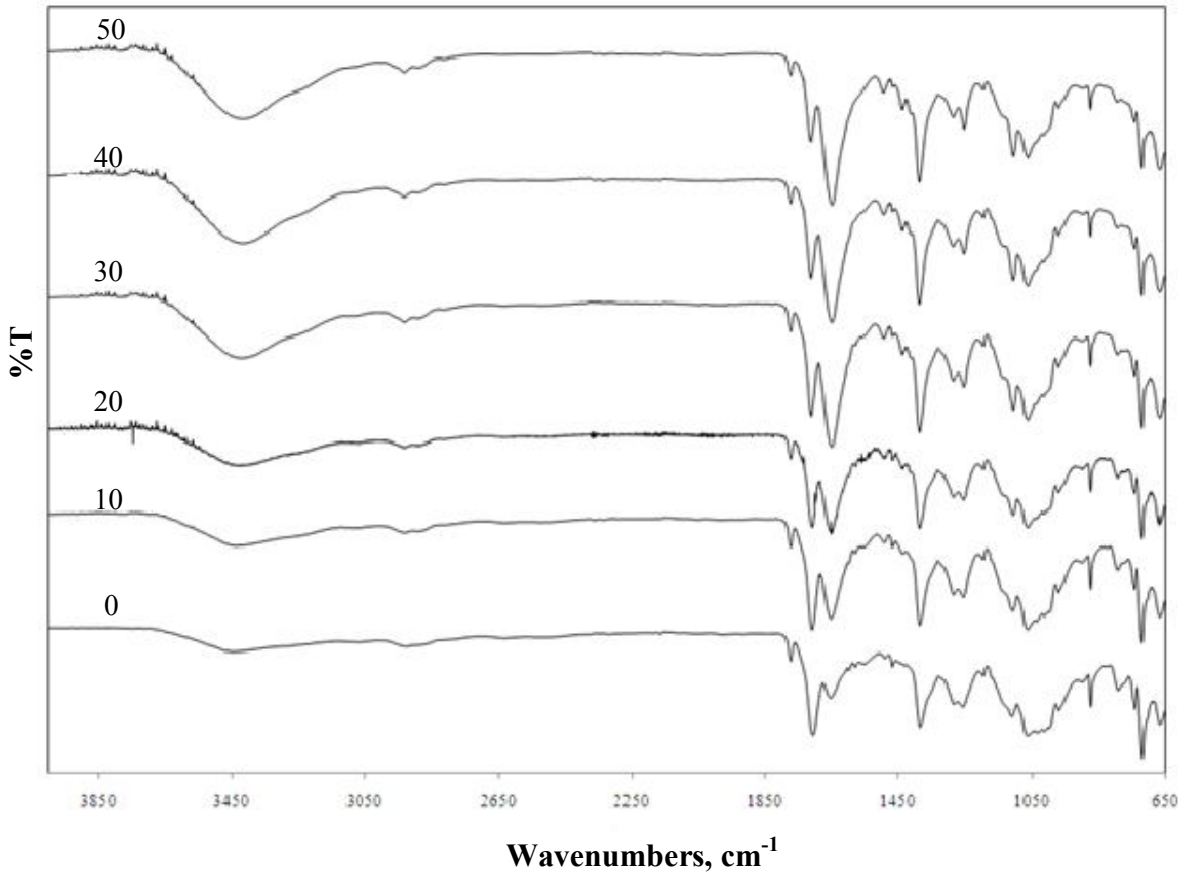

Figure 4.7: FTIR spectra of PhCh based polymer electrolytes doped with 10 to 50 wt.% of LiI

The effects of LiI salt on PhCh are shown in the phthalimido characteristic region of the FTIR spectra from wavenumber 1500 to 1800 cm^{-1}, *Figure 4.8*. After LiI salt is added, bands at 1772 and 1708 cm^{-1} attributed to phthalimido group seems to disappear. The intensity of the bands slightly decreases with increase in LiI content until 50 wt. % salt. Band at 1708 cm^{-1} shifts to 1712 cm^{-1} with increase in salt shown in *Figure 4.8*. The shift indicates that interaction might have occurred between the polymer and LiI.

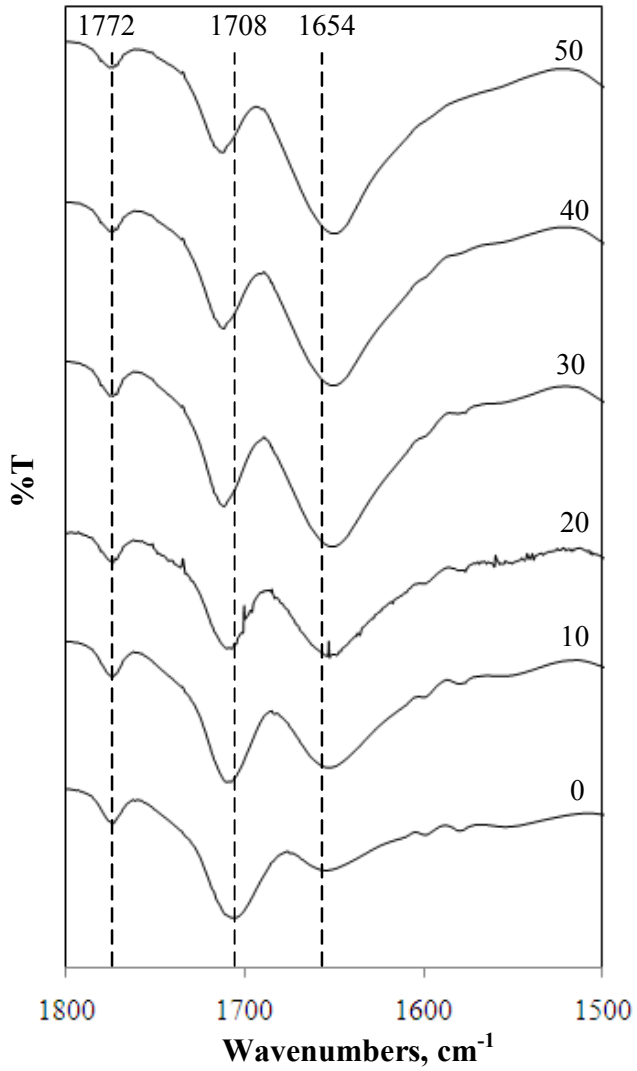

Figure 4.8: FTIR spectra of PhCh doped with various wt.% of LiI from wavenumbers 1500 to 1800 cm^{-1}

From *Figure 4.9,* the intensity of the absorption band at 719 cm^{-1} which is characteristics of an aromatic ring also decreases slightly with the addition of salt. This further shows that transformation might have taken place after LiI is introduced.

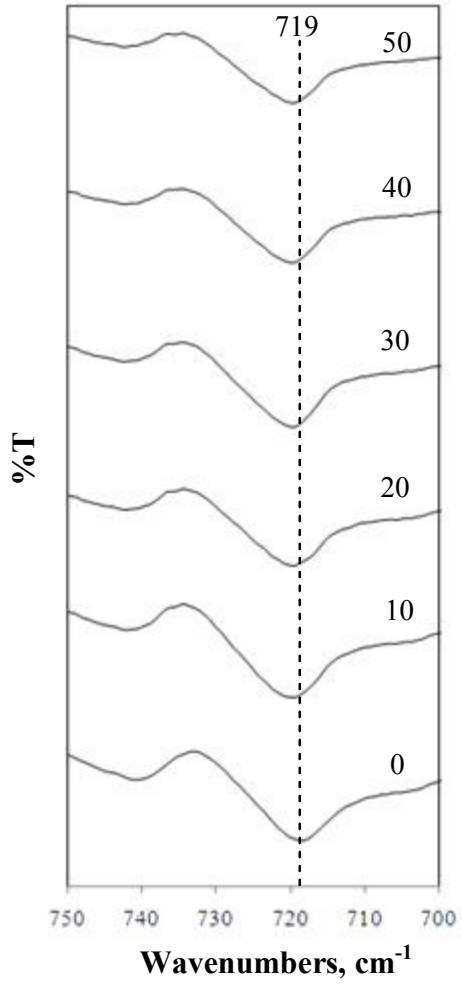

Figure 4.9: FTIR spectra of PhCh doped with various wt.% (0-50) of LiI between 700 cm^{-1} and 750 cm^{-1} wavenumbers

Consequently, a new strong absorption C=O band at 1650 cm^{-1} that is assigned to amide group appears with the addition of salt (*Figure 4.8*). The intensity of the band increases with increasing salt content. The band also shifts from 1654 cm^{-1} to 1649 cm^{-1} as salt content increase. From these observations, it is assumed that PhCh has undergone

transformation with increasing salt content. The transformation results in an amide and a carboxylic acid group. Baruah et al. [101] stated that in the presence of oxynucleophile such as water and alcohol, the ring of the phthalic anhydride can be opened either to give a dicarboxylic acid or a mono-esterified dicarboxylic acid.

In this case, there are possibilities that water might be present in the salt or from the environmental surroundings. Kurita et. al [70], also stated that alkaline condition could be harmful to the N-phthaloyl group. N-phthaloyl group was not stable under alkaline conditions and tended to decompose to some extent especially in the presence of a small amount of contaminated water. The proposed reaction mechanism of the ring opening in the presence of water is shown in *Scheme 4.5*. Water molecule acts as the oxynuclephile that will attack the carbonyl group of the phthalimido structure and forms [I^-]. After the rearrangement of the molecule, the breakage of the C-N bond happens and produces amide (N-C=O) and carboxylic acid (COOH) groups.

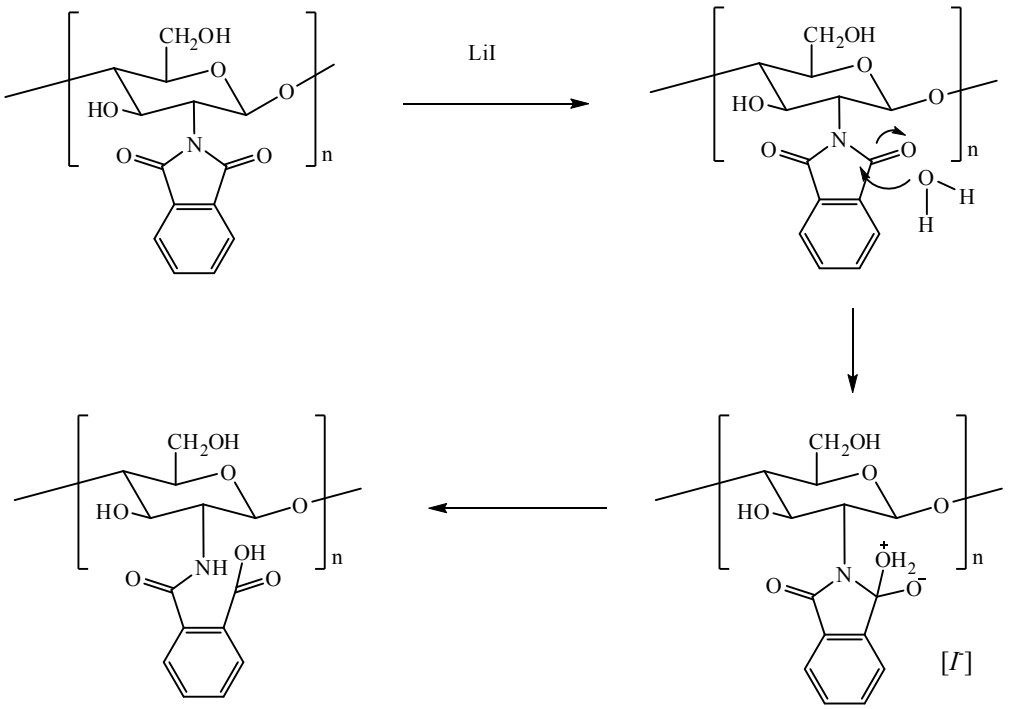

Scheme 4.5: Mechanism of hydrolysis of N-phthaloylchitosan

DMF, an aprotic solvent is not a hydrogen bond donor and has no positively charged hydrogen to form ion-dipole interaction. The molecules of an aprotic polar solvent have a partial negative charge on their surface that can solvate cations, but the partial positive charge is on the inside of the molecule, which make it less accessible (*Figure 4.10*) . The relatively "naked" anion, which is iodide ion, I^-, can be a powerful nucleophile in an aprotic polar solvent. This also explained how the addition of the LiI salt leads to the ring-opening of the PhCh to give amide and carboxylic acid groups. This argument is supported by the FTIR spectra that show changes in the bands associated to amide and carboxylic acid after salt is added as DMF has been previously mentioned to be a versatile dipolar aprotic solvent which enhances the nucleophilicity of the anions and caused the producing of amide when heated with acid chloride or anhydride [100].

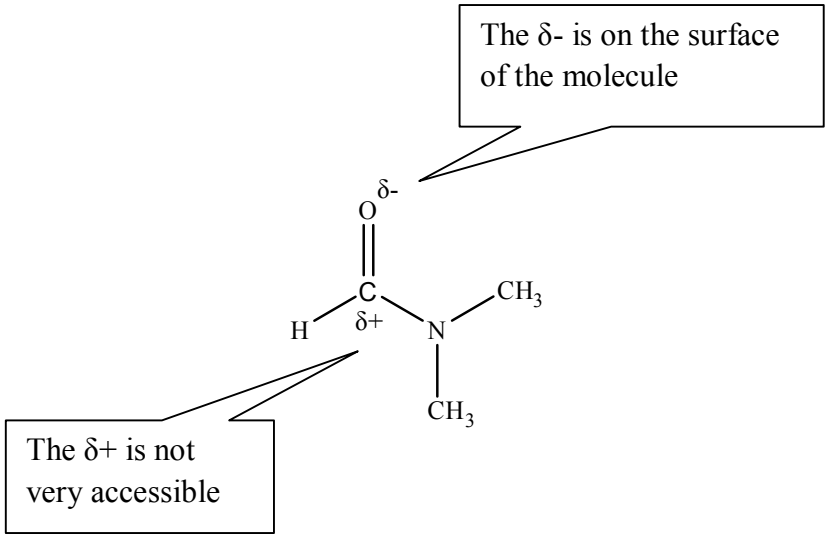

Figure 4.10: Chemical structure of DMF

Another significant peak in the FTIR spectrum region from wavenumber 3000 to 4000 cm^{-1} that changes with the addition of LiI is depicted in *Figure 4.11*. The intensity of the bands at 3450 cm^{-1} increases with the addition of LiI salt and shifts to the lower wavenumber, 3410 cm^{-1}. The band is due to an overlay of O-H and N-H bonds as both bands

stretch at wavenumbers above 3100 cm^{-1}. N-H is a band contributed by the amide group produced from the transformation of the PhCh via ring-opening and O-H band from the carboxylic acid from the ring-opening or from the water molecules that could possibly be present in the samples. Individually O-H and N-H bonds actually show different shape of absorption [59]. An N-H band is narrower and less intense than an O-H band. The O-H absorption band of a carboxylic however is broader than the O-H absorption band of alcohol. Thus, Li^+ is suggested to interact at both N atom and O atom. As strong steric hindrance is present around N atom, Li^+ might be difficult to form band with the N atom. However, O atom may also form bond with Li^+. Consequences of the above interaction lead to the ring-opening that causes the transformation of PhCh as shown in *Scheme 4.5*.

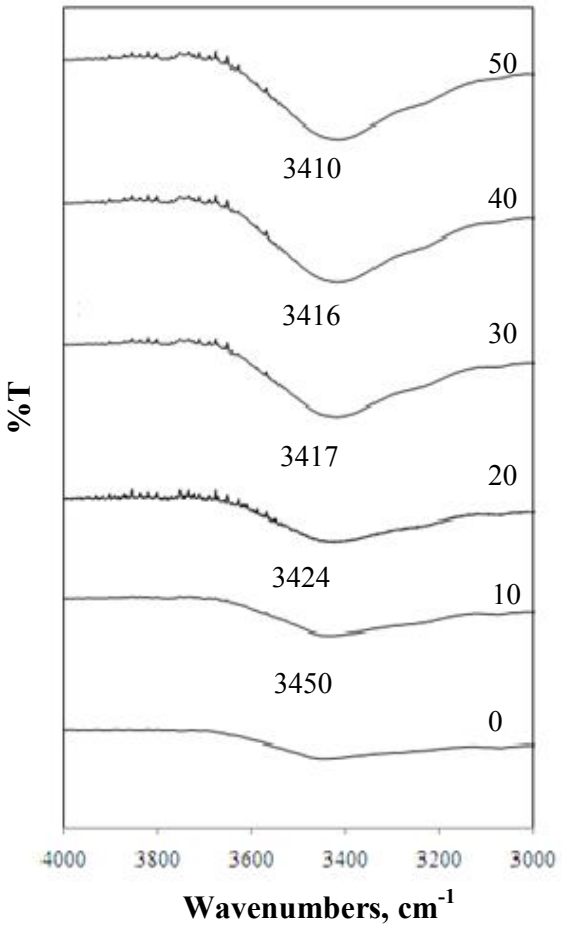

Figure 4.11: FTIR spectra of PhCh doped with LiI from wavenumbers 3000 to 4000 cm^{-1}

4.2.3. X-ray Diffractometry Analysis

XRD is one of the methods that has the advantages of strong fingerprint character and nondestruction. This method is usually used to determine the nature of the sample either in crystalline or amorphous phase. Wang et. al [102], had utilized XRD to analyze the discrepancy of *Fritillaria* that consists of plenty of starch, as the XRD spectra of the species mainly showed the crystalline properties of starch. XRD has also been employed as one of the method to confirm the complex formation between polymer and salt in polymer electrolytes [103].

Figure 4.12 shows XRD diffractograms of the doping salt, LiI used in the forming of polymer electrolytes. The nature of the salt is observed to be crystalline. High intensity peaks are obviously exhibited at 2θ angles of 21.2^{o}, 23.8^{o}, 32.1^{o}, 32.7^{o}, 42.9^{o}, 43.2^{o}, 51.8^{o} and 57.8^{o}.

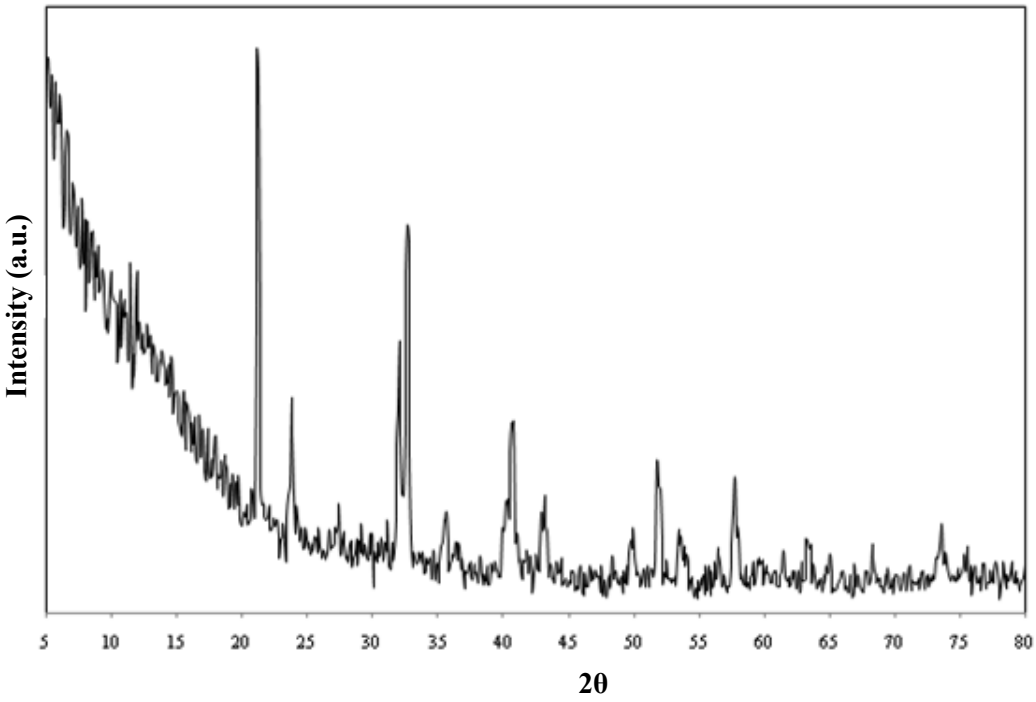

Figure 4.12: XRD diagram of lithium iodide

XRD diffractograms for phthaloylchitosan doped with LiI salt for selected weight percentages are displayed in *Figure 4.13*. A broad reflection centered at 21.1^{o} and small peak at 6.4^{o} are observed from pure phthaloylchitosan sample in agreement with previous work on other modified chitosan [74]. After 10 wt. % of LiI is added, the area under the broad peak is reduced suggesting an increase in amorphousness. Ion mobility of electroactive materials prefers amorphous state since mobile species in crystalline states are difficult to migrate due to rigid polymer chains [96]. With further increase of LiI content to 50 wt. %, intensity of the peaks are decreased. Thus, this leads to enhance ionic conductivity of the films, which is supported by the conductivity plots shown in *Figure 5.10*. All the peaks attributed to the salt have disappeared and no new peaks are observed in the diffractograms indicating that the salt is completely dissociated in the polymer matrix.

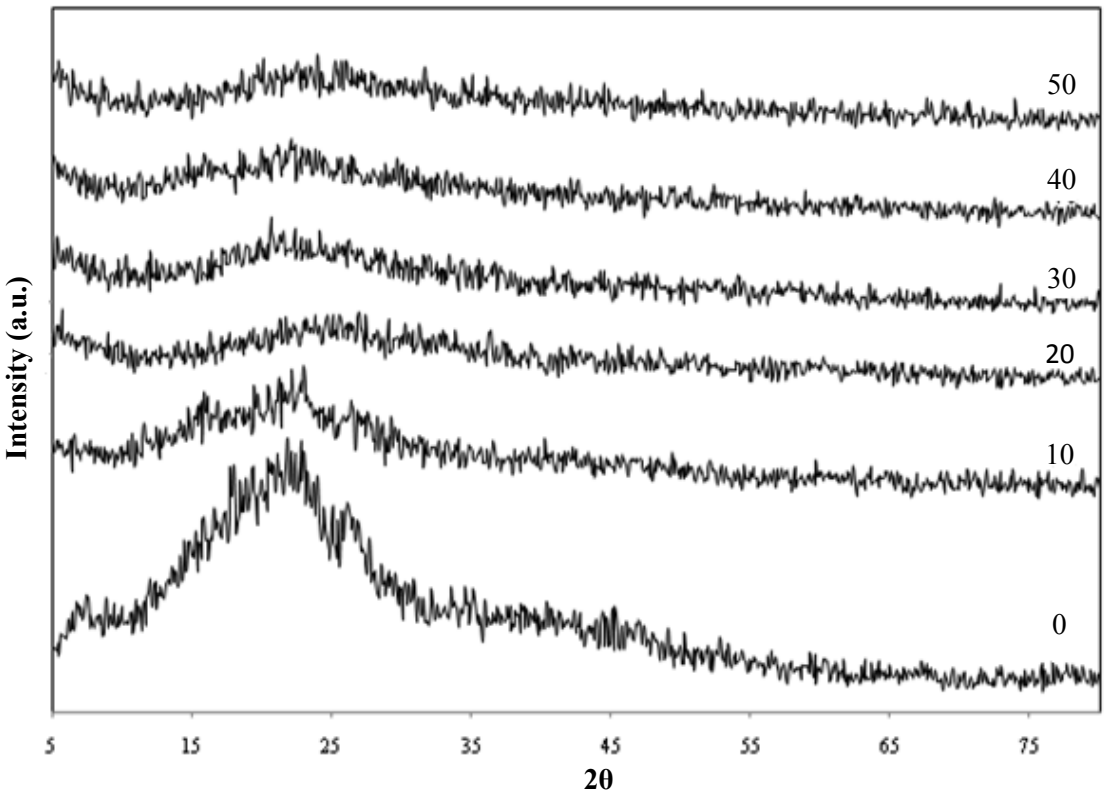

Figure 4.13: XRD diffractogram for PhCh doped with 0 to 50 wt.% of LiI films

4.2.4. Electrical Impedance Spectroscopy Analysis

4.2.4.1. Conductivity at room temperature

The continuing interest in the applications of fast ion conductors demands an improved understanding of their fundamental properties and the most directly important of which is their electrical conductivity [104]. Thus in this section, conductivity and dielectric studies will be discussed in order to see the potential of PhCh as polymer electrolyte host. The typical impedance plots of Z_r vs. Z_i for the different concentrations (0, 10, 20, 30, 40, and 50 wt.%) of LiI in PhCh-based polymer electrolyte at room temperature are shown in *Figure 4.14*. Ac impedance spectra usually show two well defined regions which are high frequency semicircle and low frequency spike. High frequency semicircle can be related to the ionic conduction process in the bulk of polymer electrolytes. However, the low frequency spike has been attributed to the effect of blocking electrode [103]. Blocking electrode is a metal electrode covered with thin dielectric layers so that no charge transfer occurs through the interface of metal electrolytes [105]. The use of the blocking electrode for the impedance spectra results in a polarization phenomenon in the solid polymer electrolytes bulk, since there is no ion source or sink [25].

Pure PhCh impedance plot shows an incomplete semicircle due to the lack of data to complete the entire semicircle. Similar pattern plot is observed for PhCh doped with 10 wt.% of LiI. After adding 20 wt.% of LiI, a complete semicircle was visible at high frequency and followed low frequency spike. The semicircle disappears after 30 wt.% of LiI addition and is followed by strong title spike. At higher concentrations of LiI salt, only low frequency spikes are visible in the plot. The semicircle disappears suggesting only the resistive component of the polymer prevails.

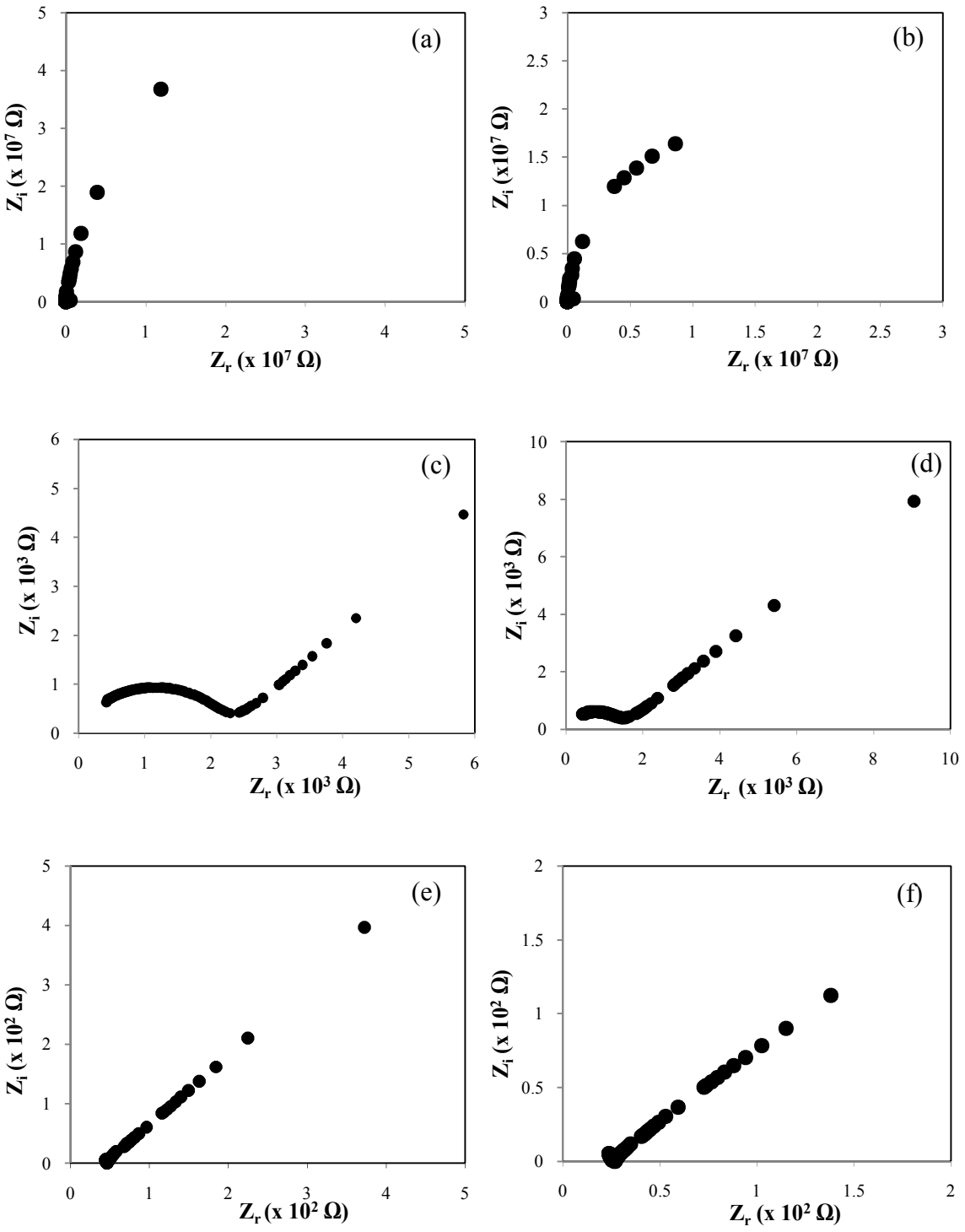

Figure 4.14: Complex impedance plots of PhCh based polymer electrolytes with (a) 0 wt.%, (b) 10 wt.%, (c) 20 wt.%, (d) 30 wt.%, (e) 40 wt.% and (f) 50 wt.% of LiI at room temperature

Bulk resistance, R_B value for the samples can be obtained from the intercept of high frequency semicircles end with the x-axis. However, in the case of PhCh with 20 and 30 wt.% of LiI, the R_B value is the intercept of the semicircle with the spike. If only spike appears on the plot as shown by PhCh – 40 wt.% LiI and PhCh – 50 wt.% LiI, the R_B value is obtained from the intercept of the real axis with the low frequency spike. The conductivity value can be calculated by inserting the R_B value into the *Equation 3.9*.

The plot of conductivity of PhCh based polymer electrolyte as a function of LiI salt concentrations at room temperature is shown in *Figure 4.15*. After 10 wt.% of LiI is added, the conductivity increases to 4.07 x 10^{-8} S cm^{-1} compared to the conductivity value of pure PhCh film which is 1.87 x 10^{-10} S cm^{-1}. The conductivity is observed to increase with LiI concentration. Values of the conductivity are also tabulated in *Table 4.5*. The highest conductivity exhibited is 1.88 x 10^{-4} S cm^{-1} for PhCh - 50 wt.% LiI. The increment in conductivity is due to the increase in number of free mobile ions [106]. This is also possibly due to the increase in the amorphousness of the polymer electrolyte with the addition of LiI salt as exhibited in XRD result in *Figure 4.13*. As LiI content increase, amorphous behavior of polymer electrolyte will increase which reduces the energy barrier (will discussed later in *Section 4.2.4.2*), thus facilitating the fast ion transport [103]. The increment of the conductivity value can also be correlated to the previous FTIR results shown in *Section 4.2.2*. The ring-opening of the phthalimido groups of PhCh giving rise to –COOH and –NCO- functional groups provides more sites for conductivity. The existence of these functional groups due to the ring-opening transformation can enhance the conductivity as there are more lone pair electrons to interact with metal salt, thus allowing the occurrence of complexation. Mishra et. al [107], studied PEO-PVA using the same salt and found that conductivity increased by four to five orders of magnitude when LiI concentration is

doubled from 10 to 20 mole %. On addition of more than 50 wt.% LiI, a free standing film cannot be formed. Thus, in this work, preparation of polymer electrolyte was stopped until 50 wt.% of LiI which exhibited the highest conductivity.

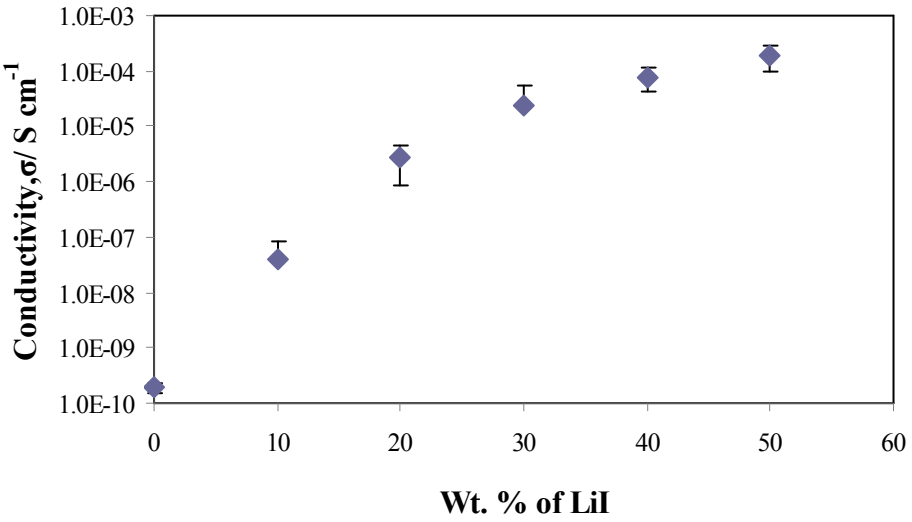

Figure 4.15: Effect of LiI concentration on the conductivity at room temperature

Table 4.5: Conductivity values of PhCh-LiI polymer electrolyte at room temperature

Sample	σ/ S cm^{-1}
PCI 0	1.87×10^{-10}
PCI 10	4.07×10^{-8}
PCI 20	2.73×10^{-6}
PCI 30	2.35×10^{-5}
PCI 40	7.80×10^{-5}
PCI 50	1.88×10^{-4}

4.2.4.2.

4.2.4.2. Conductivity vs. Temperature

The conductivity of the PhCh doped with various wt.% of LiI on temperatures is studied in order to obtain an optimum polymer electrolytes. Complex electrochemical impedances of the PhCh doped with 50 wt.% of LiI at temperature 303 K, 313 K, 323 K, 343 K, 353 K, 363 K and 373 K are shown in the Figure 4.16. The shapes of the complex impedance plots are similar with small end of the semicircle followed by low frequency spike for all the temperatures. The R_B values obtained from the intercept of the semicircles and the spikes at real axes decrease with increase in temperature. These can be observed in inset in *Figure 4.16* where the intercepts shift to the lowest number as the temperature increases.

Relationship between conductivity and temperature of PhCh doped with LiI is depicted in a plot of $log\ \sigma$ versus $1000/T$ given by *Figure 4.17*. The points are fitted to a straight line with the regression value of $0.97 < R^2 < 0.99$ as displayed in *Table 4.6*. These results indicate that the distribution of ionic conductivity with temperature for the polymer electrolytes obeys Arrhenius law, suggesting that the conductivity is thermally activated. The Arrhenius model employed in describing the temperature dependence of conductivity is as follow:

$$log\ \sigma = log\sigma_o - \frac{E_a}{kT} \tag{4.1}$$

where the σ_o is the pre-exponential factor, E_a is the activation energy of ionic conduction, k is the Boltzmann constant and T is temperature in Kelvin.

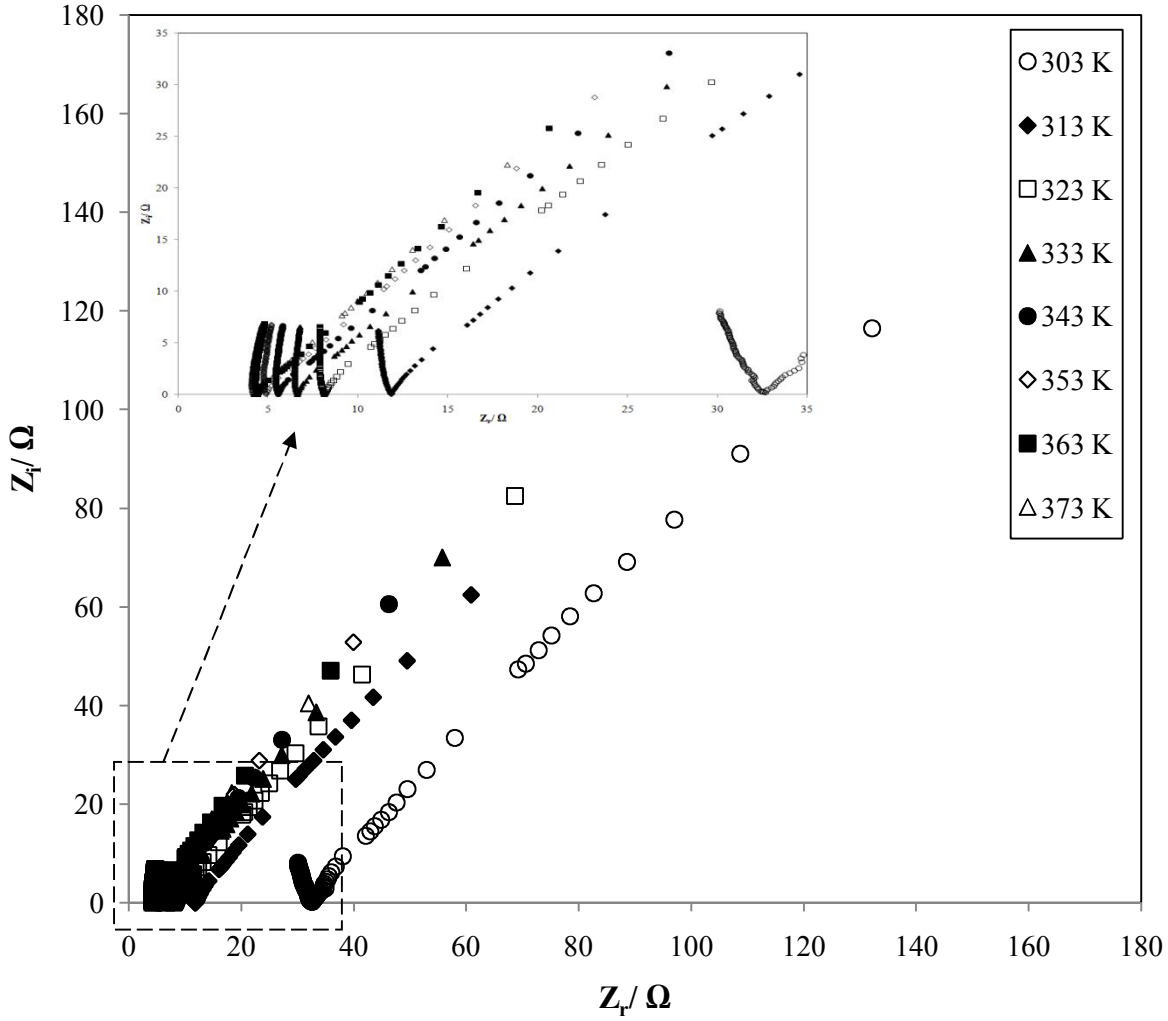

Figure 4.16: Impedance plot of PhCh doped with 50 wt.% of LiI at various temperatures.

Inset of Figure 4.16: Impedance plot between 0 and 35 Ω

From the graph of conductivity versus temperature, E_a can be calculated;

$$E_a = \frac{m \times k}{0.4342} \times 1000 \qquad (4.2)$$

where m is the value of slope and k = 8.617 x 10^{-5} eV K^{-1}.

The values of activation energy, E_a obtained are shown in the *Table 4.6* along with the ionic conductivities at room temperature. The E_a values decrease with increase in LiI concentration. Film with 10 wt.% of LiI shows the highest E_a with value of 0.5245 eV while

that with 50 wt.% of LiI has the lowest E_a value of 0.2564 eV. Lowest E_a means lowest energy barrier, thus highest conductivity. Besides low E_a value, the high conductivity may also be due to the high amorphous nature and high dissociation constant of LiI in the host polymer electric as shown in the XRD results (*Figure 4.13)*. From the Arrhenius model, it shows that when LiI salt concentration is increased, energy barrier will decrease, and consequently the ionic conductivity value will increases. This observation agrees well with the results shown in *Figure 4.15*, whereby the ionic conductivity increases with increases in wt.% of LiI.

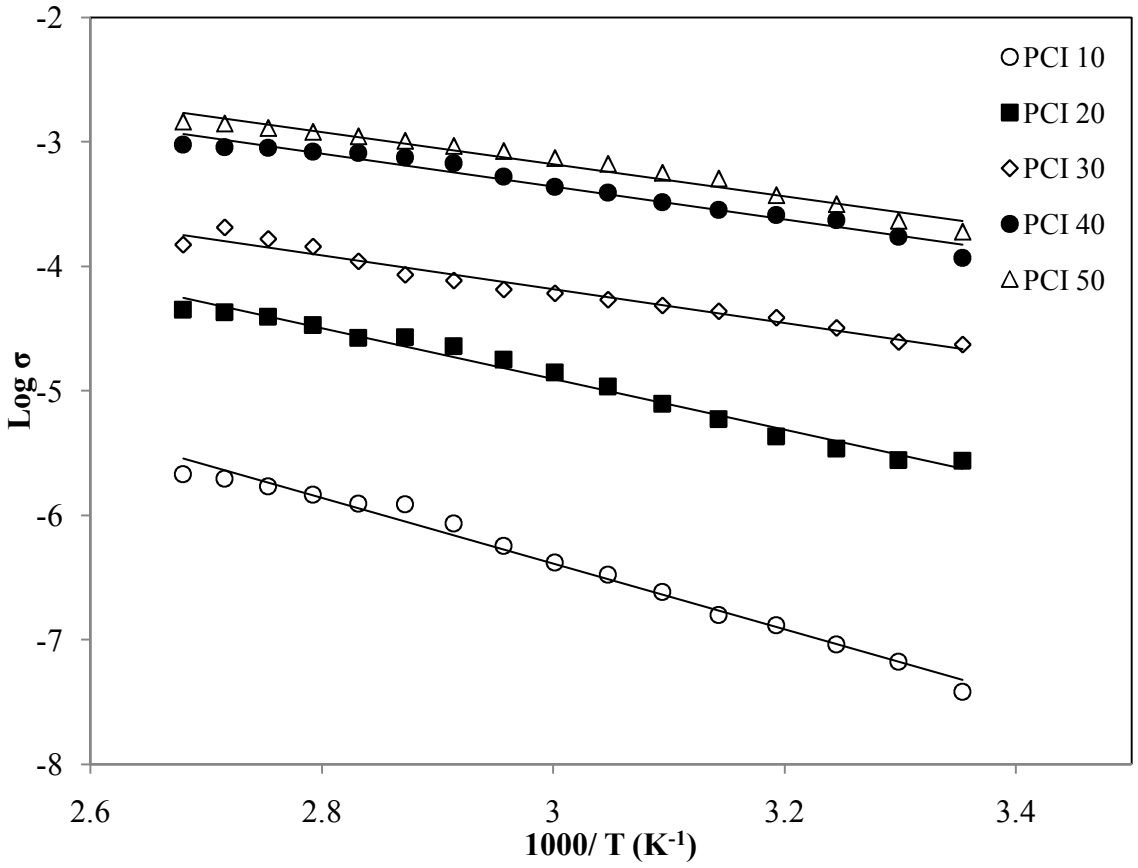

Figure 4.17: Temperature dependance of conductivity for phthaloylchitosan doped with diferent wt.% of LiI salt

Table 4.6: Ionic conductivity value of PhCh-LiI polymer electrolytes at room temperature

Sample	σ/ S cm^{-1}	R^2	E_a/ eV
PC-I 10	4.07 x 10^{-8}	0.99	0.5245
PC-I 20	2.73 x 10^{-6}	0.98	0.4037
PC-I 30	2.35 x 10^{-5}	0.97	0.2649
PC-I 40	7.80 x 10^{-5}	0.97	0.2613
PC-I 50	1.88 x 10^{-4}	0.97	0.2564

Figure 4.18 displays the relation between activation energy, ionic conductivity and salt concentrations. It is observed that the two parameters have opposite effects on weight percentage of LiI salt as has been explained earlier.

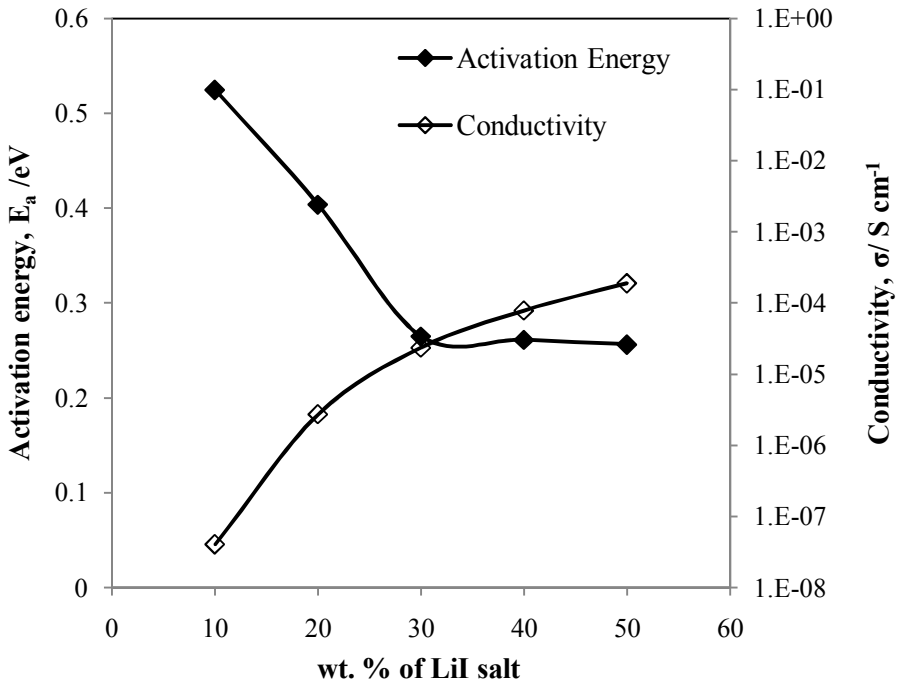

Figure 4.18: Variation of activation energy values and conductivity values as a function of wt.% of LiI salt

4.2.4.3. Dielectric studies

The study of dielectric relaxation in solid polymer electrolytes is a powerful approach for obtaining information about the characteristics of ionic molecular interactions. The dielectric parameters associated with relaxation processes are of particular significance in ion conducting polymers where the dielectric constant plays a fundamental role to show the ability of a polymer material to dissolve salt [108].

i. Electrical behavior at room temperature

Figure 4.19 presents the frequency dependent of dielectric constant, ε_r for PhCh-based polymer electrolytes with different concentrations of LiI at room temperature. ε_r can be calculated from the following equation:

$$\varepsilon_r(\omega) = \frac{Z_i}{\omega C_0 \left(Z_r{}^2 + Z_i{}^2\right)} \tag{4.3}$$

where the angular frequency, $\omega = 2\pi f$, f being the frequency in Hz and $C_0 = \varepsilon_0 A/t$ and ε_0 is the permittivity of the free space, A is the electrolyte-electrode contact area and t is thickness of the sample.

PhCh with 50 wt.% of LiI exhibits the highest ε_r plot compared to other concentrations and starts to decline with decreasing wt.% of LiI. This can be explained since the dielectric constant is a measured of stored charge [109]. As charge is carried by ions, thus it can be explained that the increase in dielectric constant reflects the increase in the number of ions. With increasing in salt content, number of charge carrier will enhance, thus lead to increasing in conductivity, as can be observed in *Figure 4.15*. Sample PhCh-50 wt.% of LiI which has the highest value of dielectric constant has the most number of ions and so has the highest conductivity value. A strong frequency dispersion of permittivity was

observed in the low frequency region followed by a nearly frequency independent behavior above 3.6 Hz. The decreasing of ε_r with increasing frequency may be attributed to the electrical relaxation processes, but at the same time the material electrode polarization cannot be ignored as the sample of our investigation are ionic conductors [110].

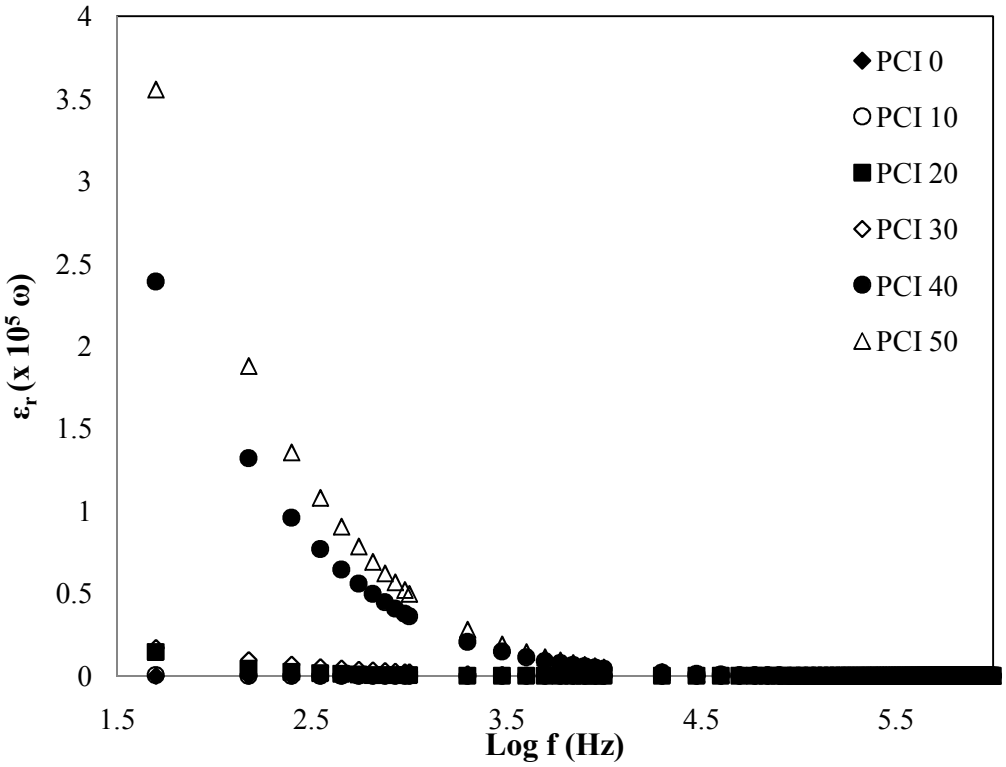

Figure 4.19: Variation of relative dielectric constant of PhCh-LiI with frequency for different concentrations of salt at room temperature

Figure 4.20 presents the frequency dependent of dielectric loss, ε_i for PhCh-based polymer electrolytes with different concentrations of LiI at room temperature. ε_i can be calculated from the equation;

$$\varepsilon_i(\omega) = \frac{Z_r}{\omega C_0 \left(Z_r{}^2 + Z_i{}^2\right)} \tag{4.4}$$

The imaginary part of permittivity plot with frequency is observed to decrease with increasing frequency. Similar pattern of ε_r has been observed as the plots declined with the

decreasing wt. % of LiI at room temperature. The higher value of ε_i at low frequency is also due to the free charge motion within the materials. At high frequencies, the periodic reversal of the electric field occurs so fast that there is no excess ion diffusion in the direction of the field. The polarization due to the charge accumulation decreases thus leading to the decrease in the value of ε_i [111-112]. There are no peaks attributed to the relaxation phenomena of polymer (motion of salt free chain segment) [28] observed in the figure. These patterns which the dielectric raise sharply at low frequencies indicating that electrode polarization and space charge effects have occurred, thus confirming non-Debye dependence [113-114].

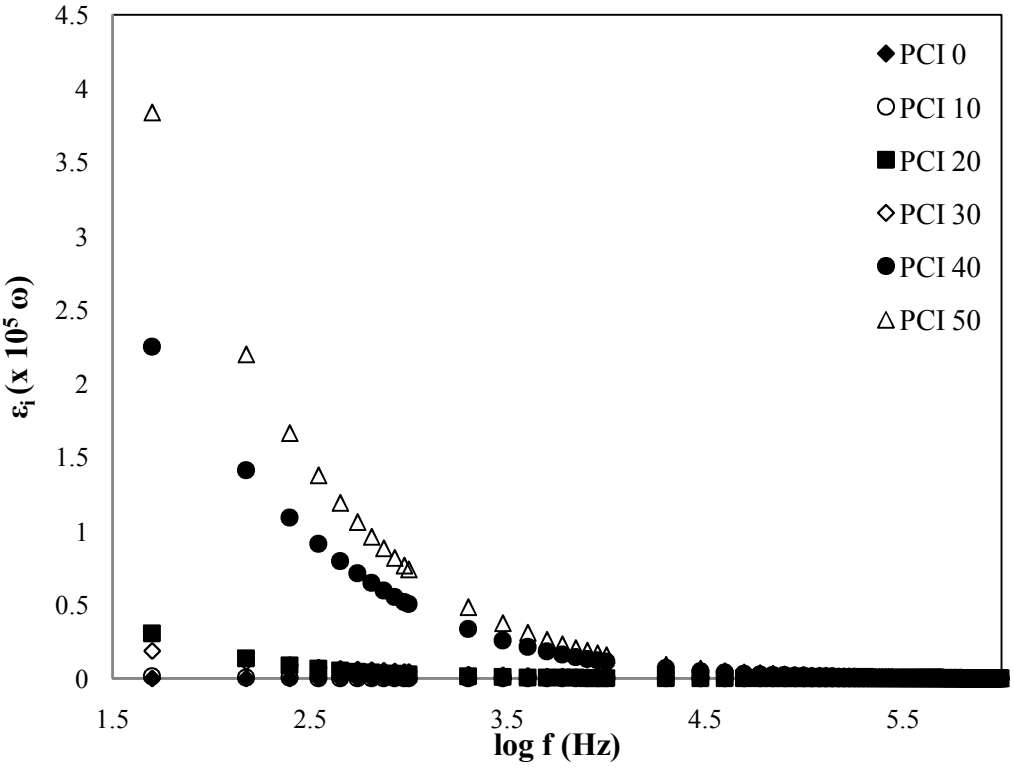

Figure 4.20: Variation of imaginary part of permittivity with frequency for different concentrations of PhCh-LiI at room temperature

The variation of real part of electrical modulus, M_r of the different LiI concentration at room temperature is exhibited in the *Figure 4.21*. M_r can be defined as;

$$M_r(\omega) = \frac{\varepsilon_r}{(\varepsilon_r{}^2 + \varepsilon_i{}^2)} \tag{4.5}$$

In the low frequency region, the M_r is observed to be independent of frequency and the values tends to zero, indicating that the contribution of electrode polarization is negligible [111]. At frequency above 3.5 Hz, a strong dispersion starts to built up. The maximum plot is shown by PhCh with the lowest wt.% of LiI of 10 wt.%, and plots decrease with increase of the LiI concentration. No well-defined dispersion peaks are observed.

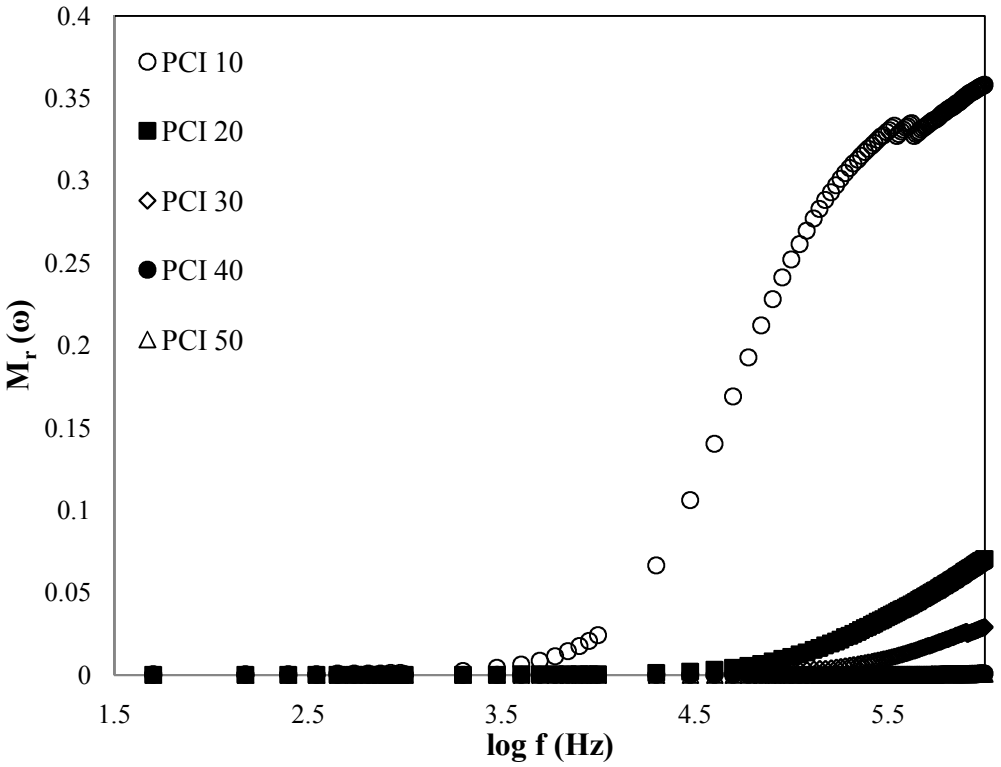

Figure 4.21: Frequency dependence of real part of electrical modulus, M_r for PhCh-LiI at room temperature

The variation of imaginary part of electrical modulus, M_i of the different LiI concentrations at room temperature however is exhibited in the *Figure 4.22*. M_i can be calculated from the following *Equation 4.6*;

$$M_i(\omega) = \frac{\varepsilon_i}{(\varepsilon_r{}^2 + \varepsilon_i{}^2)} \tag{4.6}$$

Among the plot of M_i versus frequency, only PhCh doped with 10 wt.% of LiI shows a peak at 4.7 Hz. The presence of the peak is related to the conductivity relaxation of the materials [110] thus shows that the samples are ionic conductors [115]. PhCh with 20 wt.%, 30 wt.%, 40 wt.% and 50 wt.% of LiI show the same trend with the M_r plot (*Figure 4.21*), i.e, frequency independent in the lower frequency region and begin to increase with frequency. The appearance of this long tail at low frequencies of M_r and M_i plots maybe due to the large capacitance associated with the electrodes [116]. No comparison can be made since only one significant peak is observed in the plot of M_i versus frequency.

Thus, tangent loss of PhCh-LiI films was plotted with frequency for different concentrations of LiI salt at room temperature as shown in *Figure 4.23*. Dielectric loss tangent, *tan δ*, is a dimensionless ratio of the dielectric loss to the dielectric constant;

$$tan\,\delta = \frac{\varepsilon_i}{\varepsilon_r} \tag{4.7}$$

where δ is the phase angle between the applied voltage and the current response.

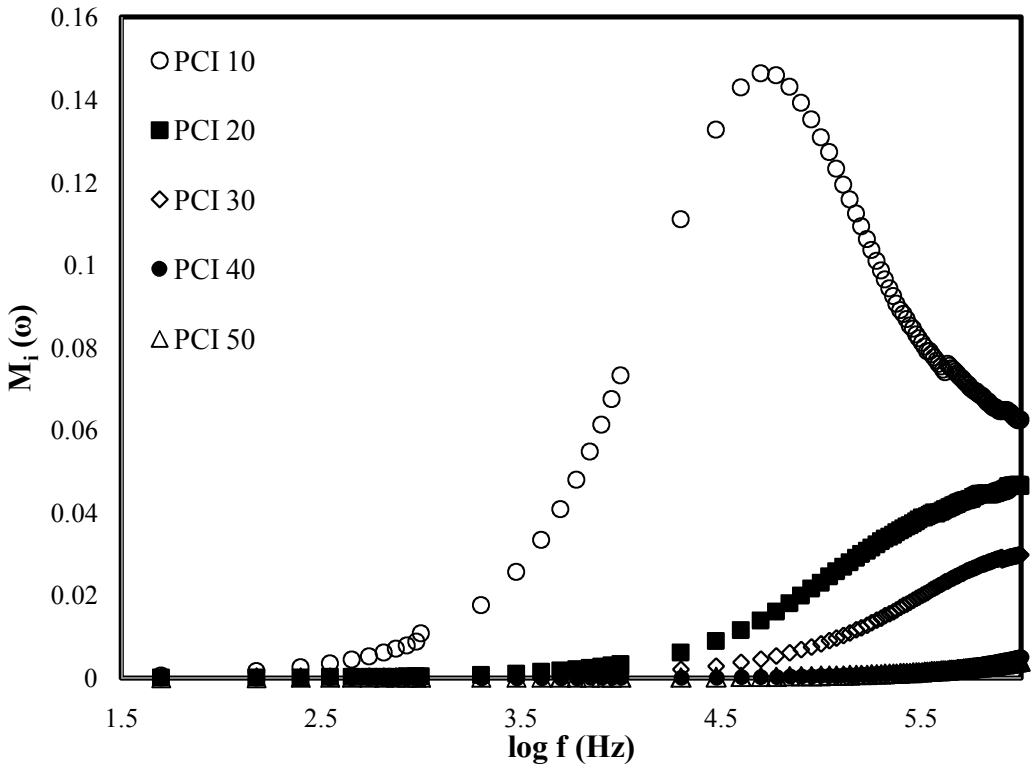

Figure 4.22: Frequency dependence of imaginary part of electrical modulus, M_i for PhCh-LiI at room temperature.

The tan loss spectra are characterized by a peak, the maximum *tan δ*, appearing at a characteristic frequency after addition of LiI salt. The *tan δ* peak shifts towards higher frequency site and the height of the peak increases with increasing in LiI concentration. The peak suggests the presence of relaxing dipoles in all the samples. The strength and frequency of relaxation depend on characteristic property of dipolar relaxation. The frequency dependent of dielectric constant and loss tangent suggest that the strength and frequency of relaxation depend on the characteristic property of dipolar relaxation. It has been observed that the peak frequency shifts towards the higher frequency side with increase in salt concentration. As the peak shifts towards higher frequency side, the relaxation time is reduced [109].

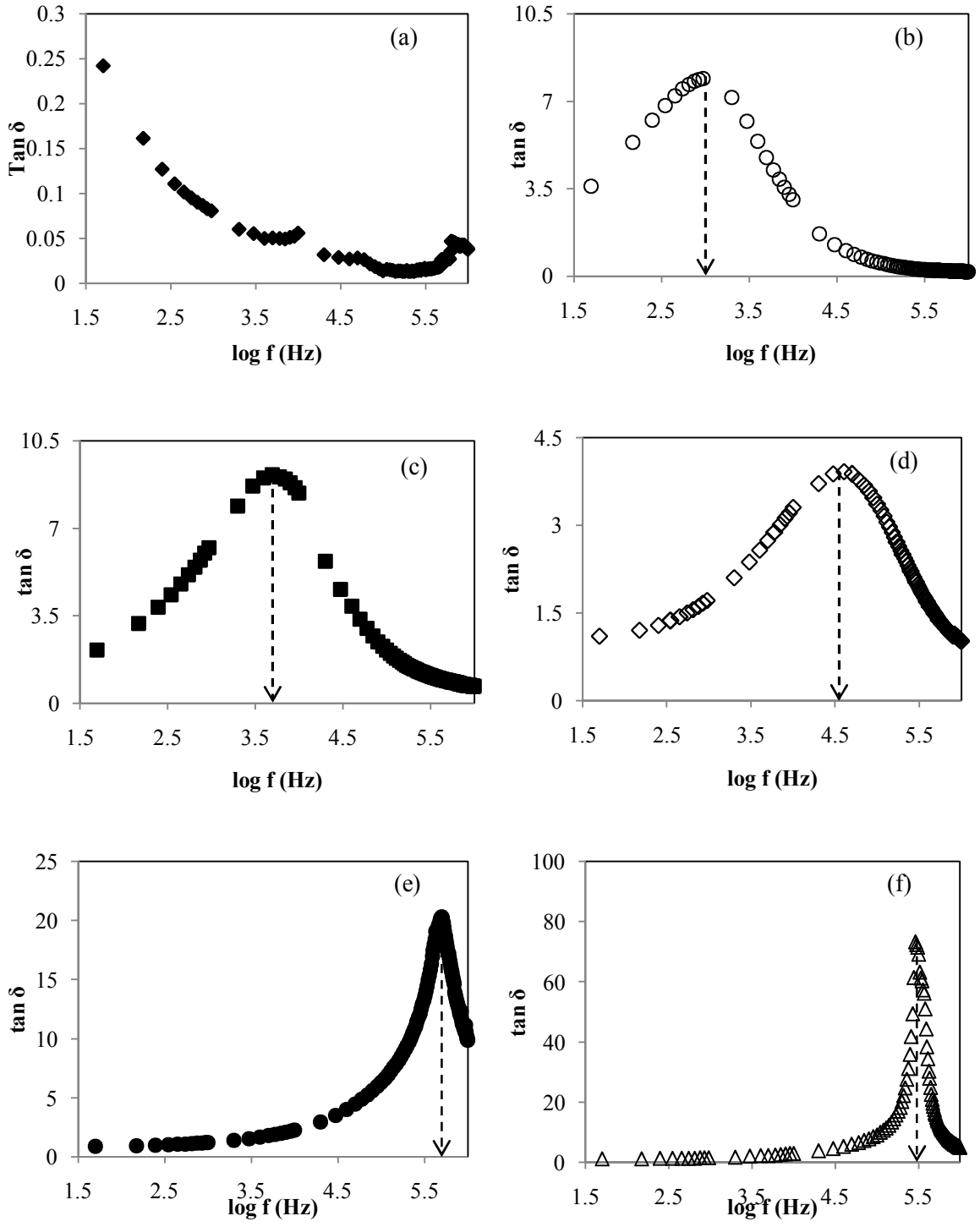

Figure 4.23: Variation of tan δ of PhCh-LiI films with frequency for different concentrations; (a) 0 wt.%, (b) 10 wt.%, (c) 20 wt.%, (d) 30 wt.%, (e) 40 wt.% and (f) 50 wt.% of LiI salt at room temperature

The angular frequency of the applied field, ω, at which the peak at the maximum of the *tan* δ, defines the relaxation time for the ionic charge carriers, τ, by the following equation:

$$\tau\omega \approx 1 \tag{4.8}$$

The effort carried out by ionic charge carriers within the polymer material to allow the change in the direction of applied field causes the presence of the relaxation time. The values of the relaxation time are exhibited in the *Table 4.7*. From the tabulated data, relaxation time is observed to decrease with the increasing of wt.% of LiI.

Table 4.7: Relaxation time of various concentrations of LiI in PhCh based polymer electrolyte at room temperature

Wt. % of LiI	ω	T
10	5969.8	1.68E-04
20	62840.0	1.59E-05
30	691240.0	1.45E-06
40	1319640.0	7.58E-07
50	1948040.0	5.13E-07

The dependence of conductivity and relaxation time on concentrations of LiI in the PhCh polymer electrolytes is shown in *Figure 4.24*. The effect of the conductivity is inversely proportional to the relaxation time with respect to the concentration of LiI. As the conductivity increases with increasing LiI content, the relaxation time decreases.

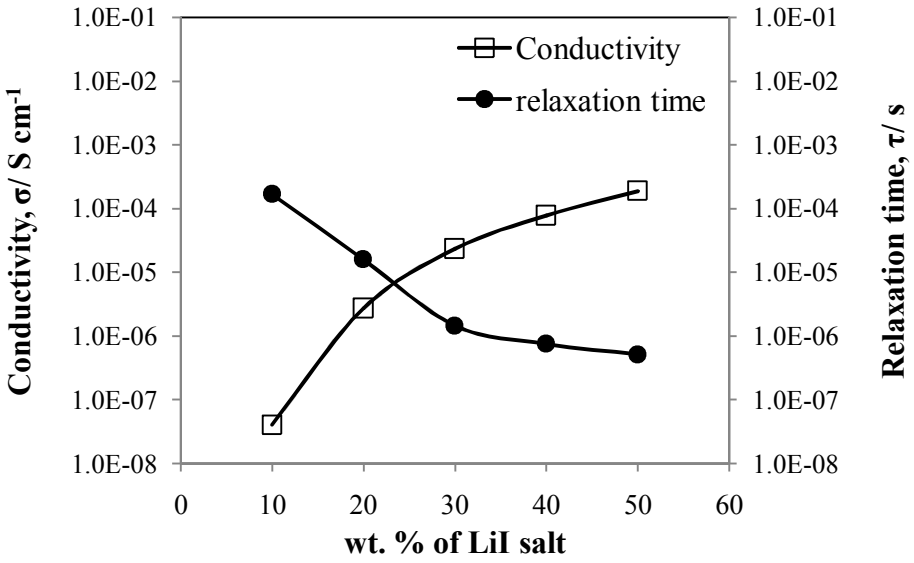

Figure 4.24: Variation of conductivity and relaxation time of different salt concentrations of LiI in PhCh based polymer electrolytes at room temperature

Dielectric studies of the PhCh-LiI are further discussed with the dependence of the ac conductivity with frequency for different concentrations of LiI at room temperature as shown in *Figure 4.25*. The ac conductivity was calculated from the following equation:

$$\sigma_{ac} = \frac{Z_r}{({Z_r}^2 + {Z_i}^2)} \times \frac{t}{A} \tag{4.9}$$

where t is the thickness of the film and A is the film-electrode contact area.

The conductivity increases with increases in frequency. It can be observed that at low frequencies, the conductivity value is low. The conductivity then increases gradually as the frequency increases. The low conductivity value at low frequencies is related to the accumulation of ions due to the slow periodic reversal of the electric field [109].

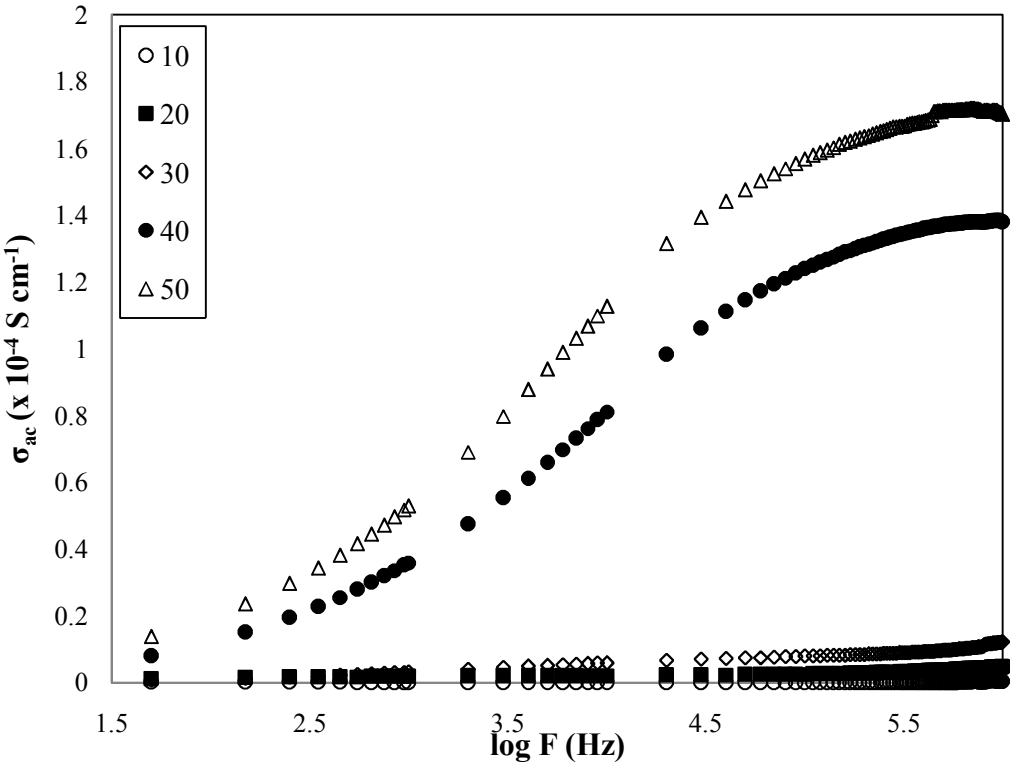

Figure 4.25: Variation of ac conductivity with frequency of polymer electrolytes at room temperature

ii. Dielectric behavior at different temperatures

The dielectric behavior of PhCh based polymer electrolytes doped with 50 wt. % of LiI (the most conducting sample) has been studied for temperature range from 303 K to 373 K. It is generally believed that dielectric data is characterized by superposition of two processes which are, (i) conductivity contribution that produces an increase of both real part ε_r and the imaginary part, ε_i of the dielectric function on decreasing frequency and (ii) a relaxation process exhibiting a maximum in ε_i that shifts to higher frequency side with increase in temperature [28].

Frequency dependence of dielectric constant and dielectric loss at various temperatures are shown in *Figure 4.26* and *Figure 4.27*, respectively. A variation of temperature has the effect of shifting the permittivity data along with the frequency scale with only a slight change of the vertical scale. The plot observed fall on a regular line which tends to ω dependence at lower frequencies and shows a slight slope at the higher end [104]. The low-frequency behavior is consistent with the observed trend in a wide range of materials with significant charge carrier densities contributing to polarization. A rapid decrease in ε_r and ε_i at the low frequency may be attributed to the tendency of dipoles in macromolecules to orient themselves in the direction of the applied field thus leading to a lag between the frequency of oscillating dipole and cause the value of the dielectric constant to decrease rapidly [103,108].

It can be observed from both figures that ε_r and ε_i plot of samples containing 50 wt. % of LiI in PhCh based polymer electrolytes increase with temperature. This is due to the higher charge carrier at higher temperature. As temperature increases, the degree of salt dissociation and redissociation of ion aggregates increases resulting in the increase in number of free ions or charge carrier density [109]. This is comparable to the ionic conductivity trend shown in *Figure 4.17* as conductivity increase with temperature.

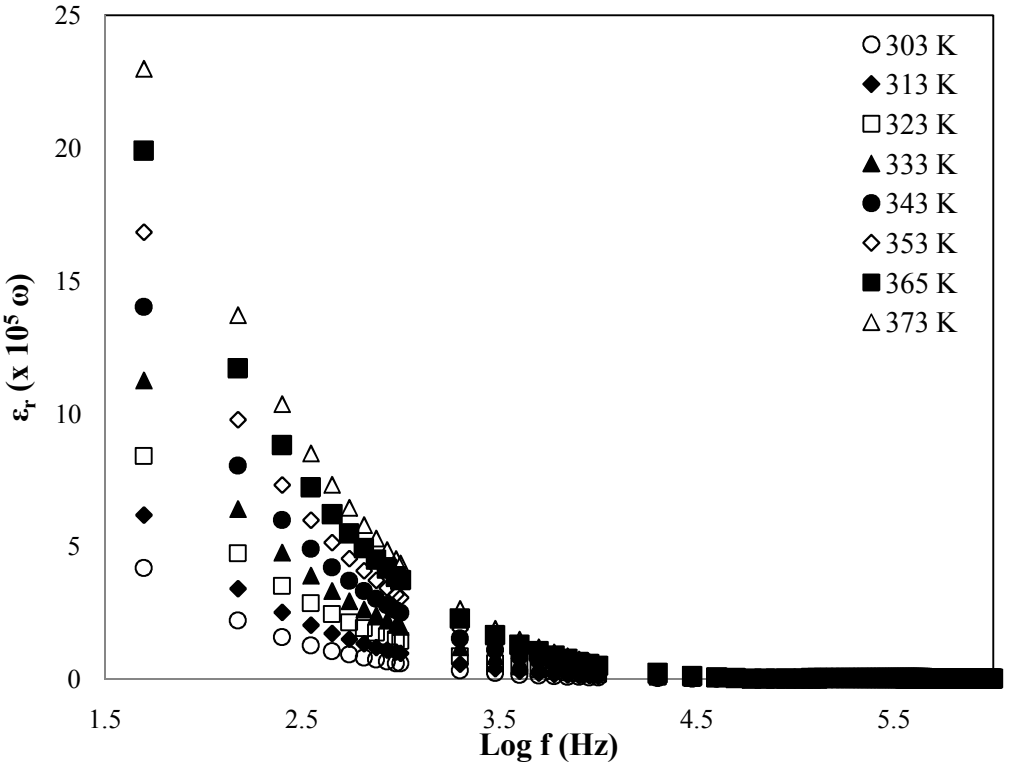

Figure 4.26: Variation of real part of permittivity with frequency for different temperature of PhCh based polymer electrolytes doped with LiI

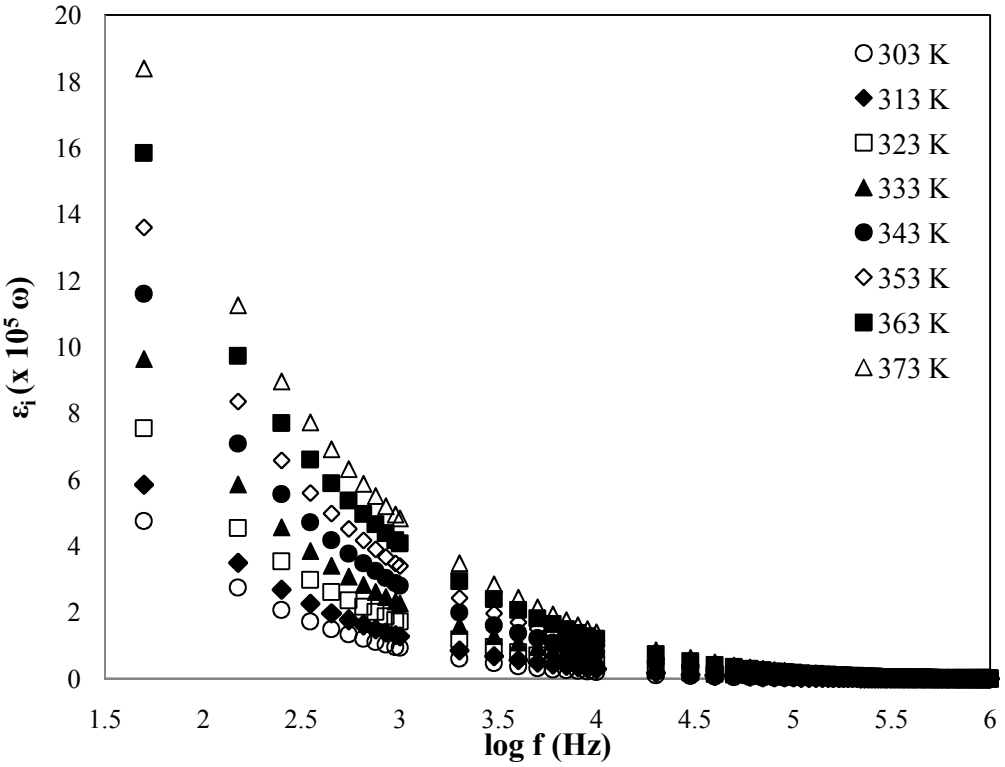

Figure 4.27: Plot of dielectric loss with frequency for PhCh-50 wt.% of LiI polymer electrolytes at temperature 303 K to 373 K

Variation of real part and imaginary part of electrical modulus, M_r and M_i, with the function of frequency at various temperatures are exhibited in *Figure 4.28* and *4.29*, respectively. The patterns of M_r plots are almost similar for every temperature. The points are constant at the beginning and started to increase dramatically towards the frequency end. The long tail at the low frequency region may be attributed to the large capacitance associated with the electrode [103].

The same observation is also seen in *Figure 4.29*. The increment of M_i value starts around 4.0 Hz. Temperature 303 K shows the highest plot and the plot decreases with increasing of temperature. An increase in M_r and M_i at high frequency end has been observed which is attributed to the bulk effect [111]. No peak is observed in both electrical modulus distributions. Therefore, tangent loss data is presented with respect to frequency for PhCh-LiI.

Frequency dependence of tangent loss at various temperatures from 303 K to 373 K for PhCh-50 wt.% of LiI was exhibited in *Figure 4.30*. Peaks are observed in characteristic frequency for every temperature indicating that the presence of relaxing dipoles in all the samples. The strength and frequency of relaxation depend on characteristic property of dipolar relaxation [28]. With increasing of temperature, the tangent loss peaks shift towards the higher frequency side. This is due to the increment in number of charge carriers for conduction which decreased the resistivity of the sample. The electric field relaxation due to the motion of ions is generally described by Kohlrausch function [20].

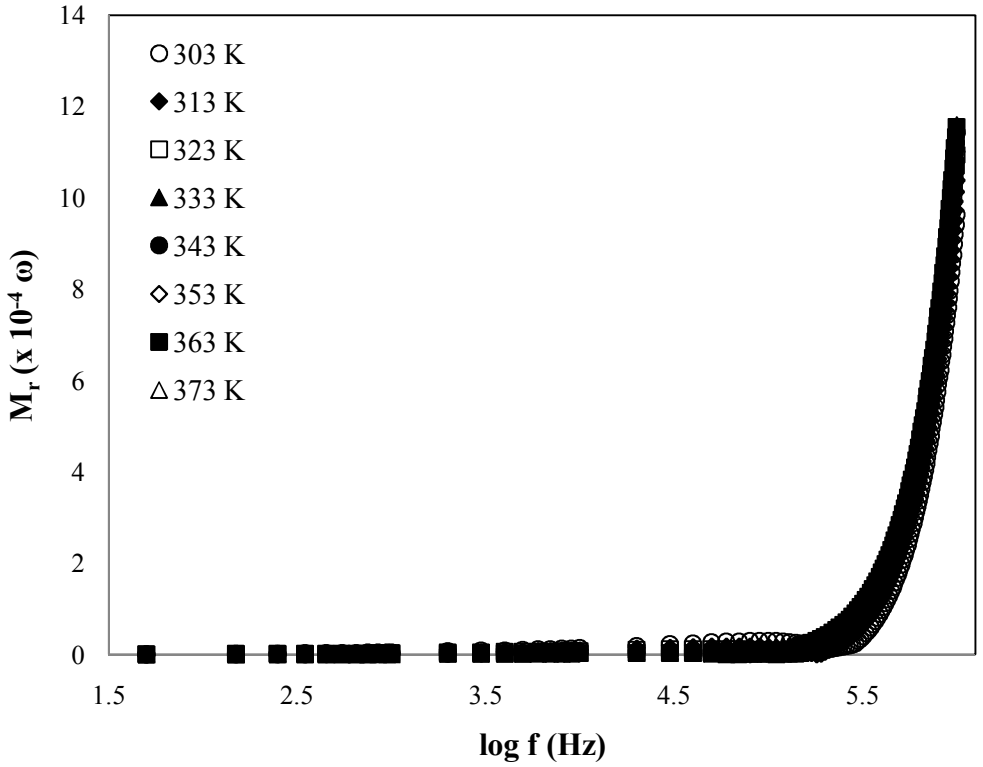

Figure 4.28: Frequency dependence of real part of electrical modulus, M_r at various temperatures for PhCh-50 wt.% LiI

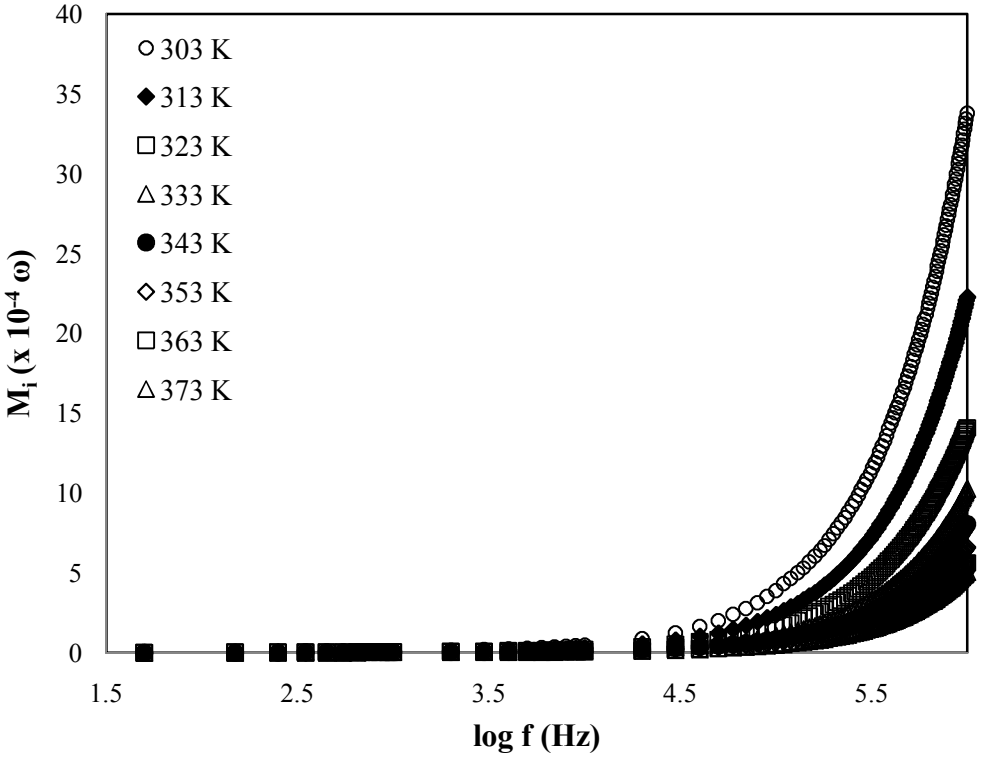

Figure 4.29: Frequency dependence of imaginary part of electrical modulus, M_i at various temperatures for PhCh-50 wt.% LiI

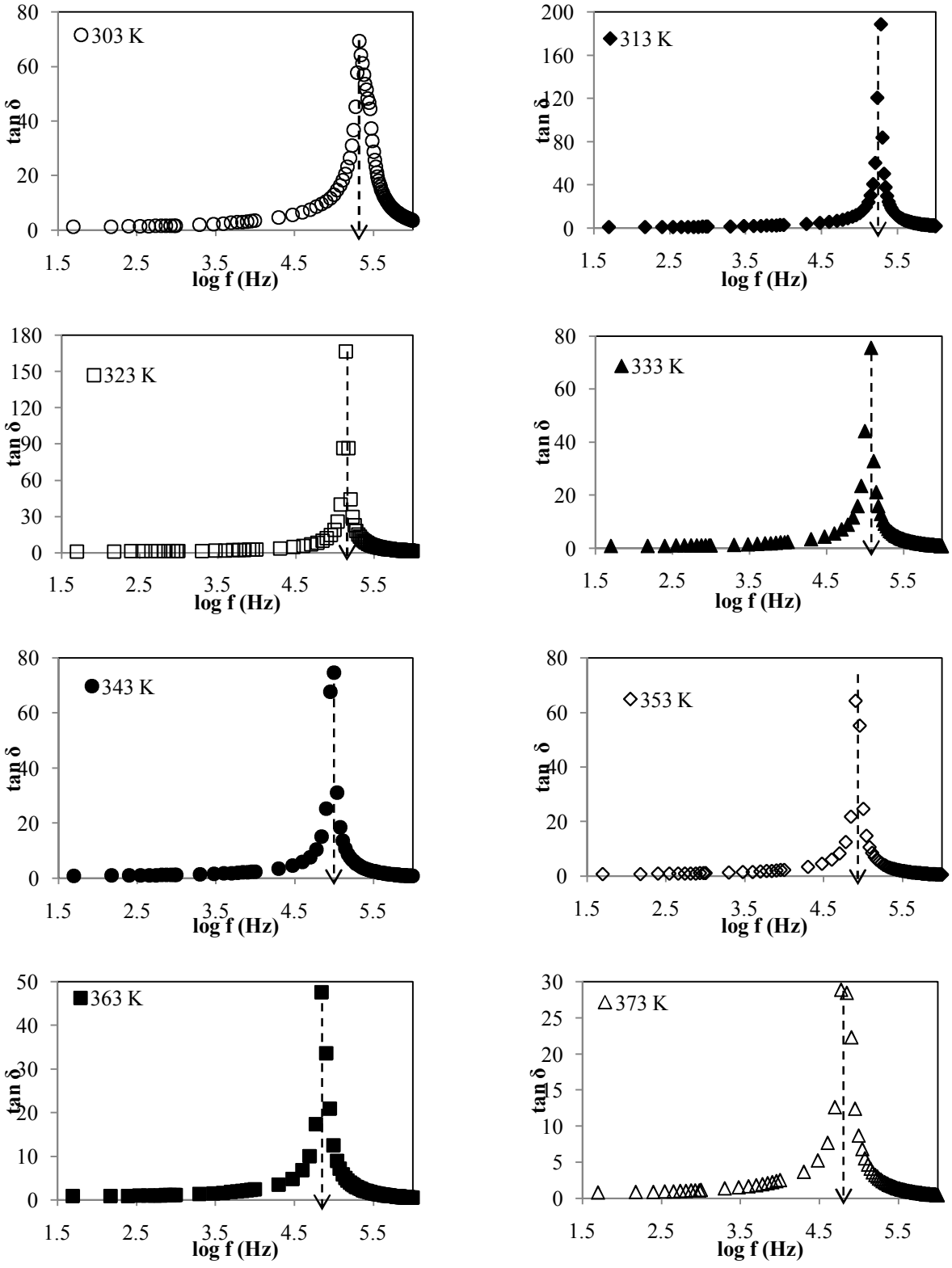

Figure 4.30: Variation of loss tan δ with frequency for PhCh-50wt.% LiI at selected temperatures

The conductivity relaxation can be described by the Kohlrausch-Williams-Watts (KWW) law stretched exponent function:

$$\Phi = \exp\left[\left(\frac{-t}{\tau}\right)^{\beta}\right] \tag{4.10}$$

where τ is the characteristic relaxation time and β is the Kohlrausch exponent. β can be obtained from the following equation:

$$\beta = \frac{1.14}{FWHM} \tag{4.11}$$

The full-width at half maximum (FWHM) of *tan* δ versus frequency were measured using Origin50 software.

From the *Table 4.8*, it can be seen that FWHM values decrease with increase in temperature, from 22.022 at temperature 303 K reduced to 8.906 at temperature 373 K. The β values also decrease with increase in temperature. The low β values obtained suggest significant stretching of the relaxation time. The origin of the low values of β can be attributed to a significant spread in the energy states of Li^+ ions in the polymer electrolytes. In addition, the smaller value of β means the larger deviation of the relaxation with respect to a Debye-type relaxation ($\beta = 1$) [20].

Relaxation time can be calculated from the ω of the peak of *tan* δ, ω_{peak} using the *Equation 4.12*:

$$\tau = \frac{1}{\omega_{peak}} \tag{4.12}$$

The distribution of relaxation time with temperature is shown in *Figure 4.31*. The value of τ is observed to decrease with decrease in temperature.

Table 4.8: FWHM and β values of PhCh-50 wt.% LiI at various temperatures

Temperature/ K	Peak position/ cm^{-1}	FWHM	β
303	5.322	22.022	0.052
313	5.278	19.335	0.059
323	5.146	14.061	0.081
333	5.079	11.544	0.099
343	5.000	10.700	0.107
353	4.903	10.204	0.112
363	4.845	9.234	0.123
373	4.778	8.906	0.128

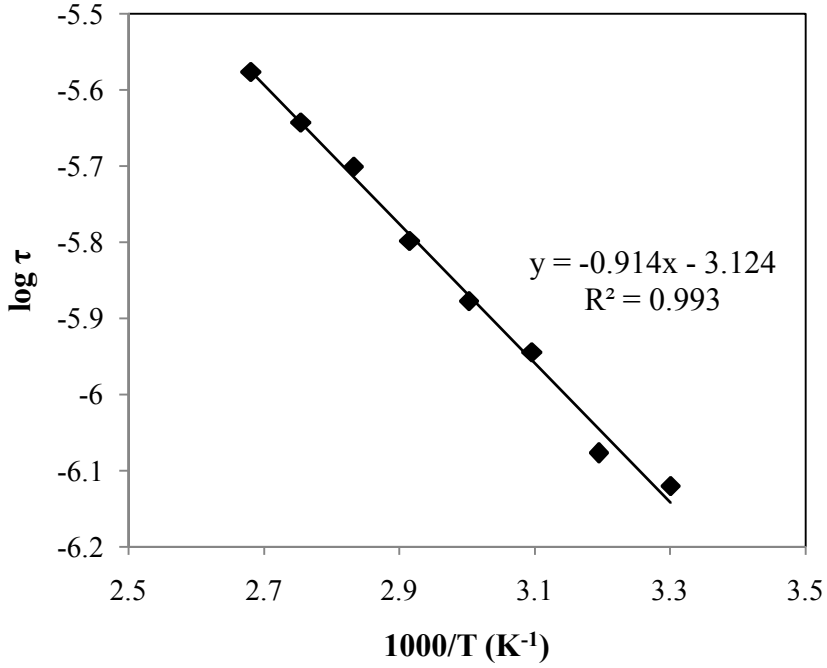

Figure 4.31: Temperature dependence of relaxation time, τ of PhCh-50 wt.% of LiI

Frequency dependence of AC conductivity for the PhCh-LiI polymer electrolytes at various temperatures are shown in *Figure 4.32*. It can be observed that the conductivity increases gradually as frequency increases. The low–conductivity value at low frequencies is related to the accumulation of ions due to the slow periodic reversal of the electric field [109]. At low frequencies, ions travel much slower and so are able to jump from one site to another vacant site.

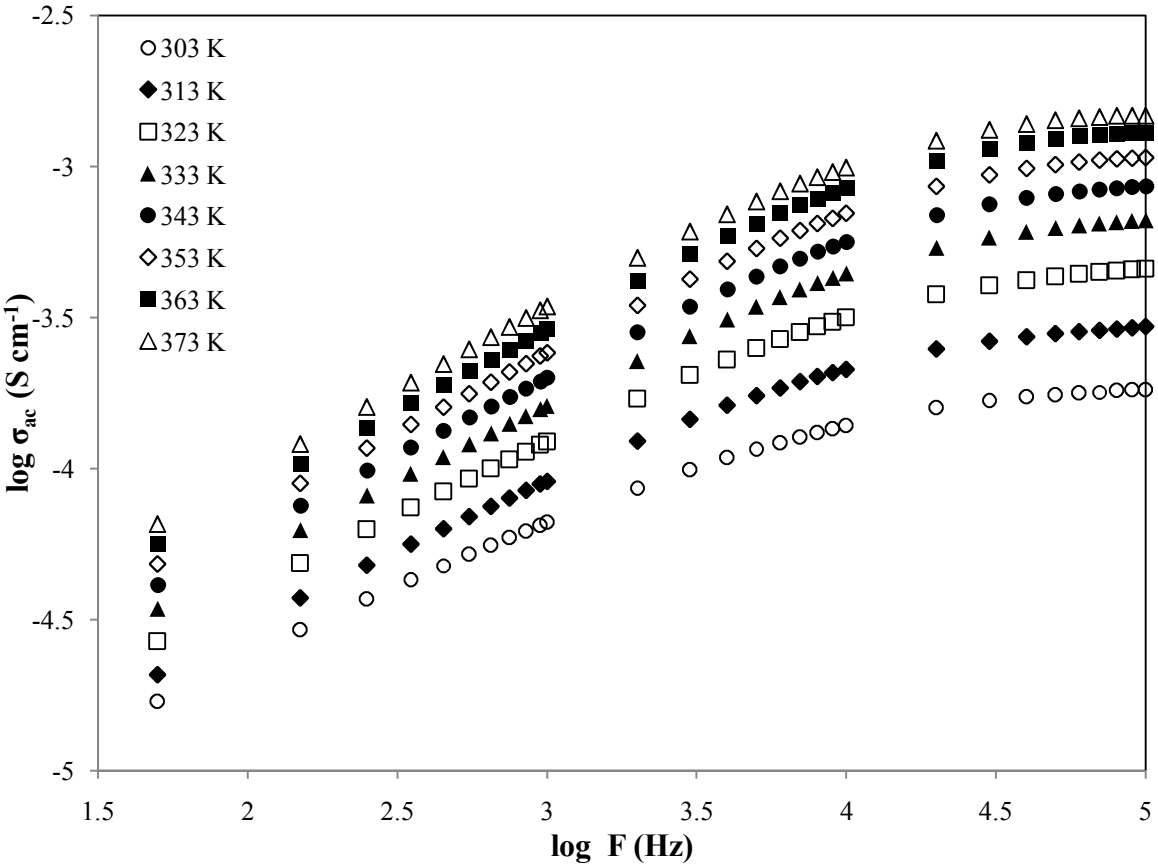

Figure 4.32: Variation of ac conductivity of PhCh with frequency at different temperatures

Studies on the dielectric behavior of PhCh complexes clearly show that the values of dielectric parameters, ε_r, ε_i, M_r, M_i, *tan* δ and σ_{ac} are strongly dependent on the frequency and also temperature, thus related to the conductivity.

4.3 Dye-sensitized Solar cell

Film with the highest conductivity value containing 50 wt. % of LiI, was applied in the dye-sensitized solar cell. In this work, natural dye was used instead of the synthetic sensitizer, ruthenium polypyridyl complexes, which is harmful to the environment, complicated to synthesize and is also costly. The natural dye in this work has been extracted from black rice and red cabbage. The color of the dye extracted from black rice is purplish-red and from red cabbage is reddish-maroon.

4.3.1. Performance of DSSC Using Dye From Black Rice

The photovoltaic tests of DSSC using natural dye extracts as sensitizer were carried out by measuring the I-V characteristic curves under irradiation with light source from 100 mW Xe arc lamp at room temperature. The current-voltage characteristics of the cells for different pH values of the extracted dye from black rice are shown in *Figure 4.33*. Performance of the DSSCs is reflected from the parameters of the I-V curves including short circuit photocurrent (I_{SC}), open-circuit voltage (V_{OC}), fill factor (FF) and energy conversion efficiency (η) as shown in *Table 4.9*.

J_{SC} is the current flows with zero external resistance (V=0) and the maximum current delivered by the DSSC while V_{OC} is the potential that develops across the terminals of the solar cell when the external load resistance is very large. Acid-untreated dye with pH 5 shows the highest curve compared to other acid-treated dye with the highest value of J_{SC} and V_{OC} corresponding to 0.34 V and 1.63 mA cm^{-2}, respectively. However, the most efficient DSSC is performed by dye at pH 2 with the value of 0.18 %. One common measure of the quality of a solar cell or module is its efficiency. In general, efficiency is defined as the ratio

of output from a device compared to the input to the device. In this work, active area efficiency refers to a single cell and only includes the active semiconductor area of the cell, i.e. 0.25 cm^2. Beside efficiency, *FF* is also the key parameter in evaluating the performance of solar cells. Fill factor in the context of solar cell is defined as the ratio of the actual maximum obtained power (V_{max} x I_{max}) to the theoretical power (which is actually not obtainable), (J_{sc} x V_{oc}). Typical commercial solar cells have a fill factor > 0.70. Grade B cell, have a fill factor in a range of 0.4 and 0.7 [117]. pH 2 also shows the highest *FF* value of 0.44 followed by pH 1 with 0.43. At lowest pH of 0.5, the DSSC gives the worst performance with 0.01 % of energy conversion efficiency.

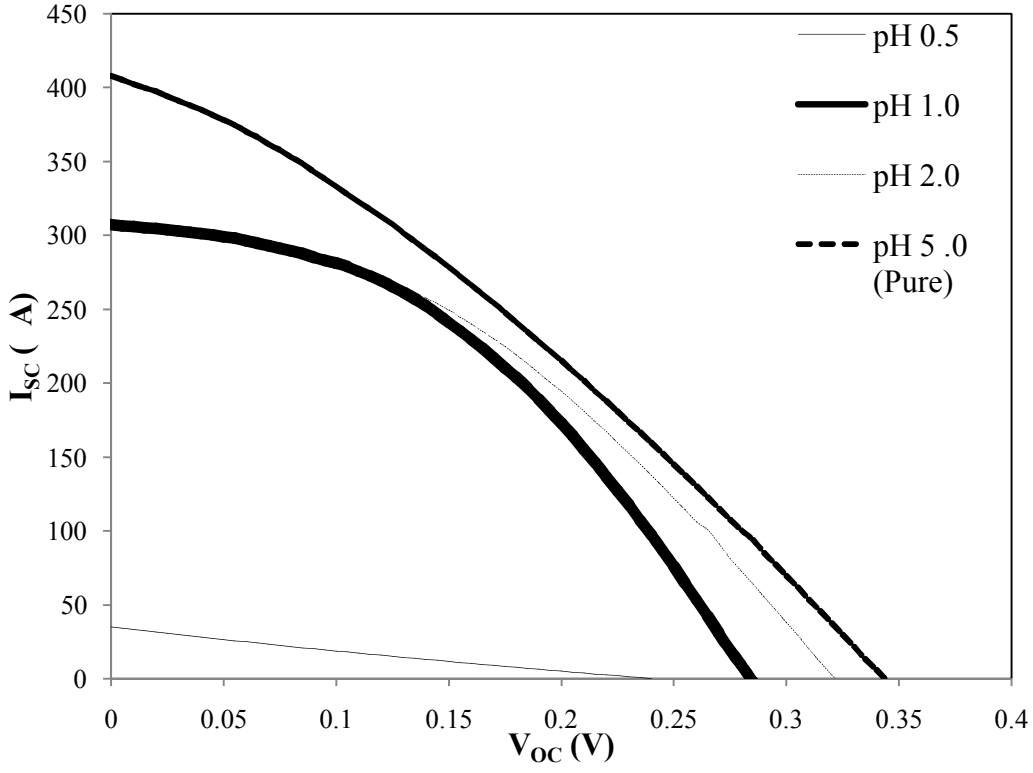

Figure 4.33: Current-voltage curves of DSSC using extracted dye from black rice

Table 4.9: Performance of DSSCs using dye extracted from black rice with various pH

pH of dye	V_{OC}/ V	I_{SC}/ mA	J_{SC}/ mA cm^{-2}	*FF*	η/ %
0.5	0.24	0.04	0.16	0.22	0.01
1.0	0.28	0.31	1.24	0.43	0.15
2.0	0.32	0.31	1.24	0.44	0.18
5.0	0.34	0.41	1.63	0.31	0.17

From the spectra in *Figure 4.34*, we can observe that the absorbance of the pigment solutions is pH dependent. It has been reported that absorption band of anthocyanin is pH and solvent sensitive. The absorption peak of dye extracted from black rice lies at the wavelength between 531 and 533 nm. This might be due to the fact that dye extracted from black rice with pH 1 can absorb more light compared to other pHs, indicated by peak intensity shown in *Figure 4.34*.

Anthocyanin is actually a colorless compound because it does not absorb visible light. In acidic environment, the -OH group becomes protonated and water is eliminated. Loss of water results in the heterocyclic ring becoming conjugated with the rest of the molecule. As a result of the extended conjugation, the anthocyanin absorbs visible light with wavelengths between 480 nm and 550 nm [22]. In acidic solution, it will show red flavylium form ($TiA^{+}H$) and purple deprotonated quinonodial form (TiA) as pH increases [80]. According to Bakowska et. al, at pH below 2, anthocyanin exists as flavylium ion, the stable form of anthocyanin and increasing the pH will hydrated this ion to quinonoidal bases. These compounds are labile and can be transformed into colorless carbinol pseudobase and chalcone [56,80] as shown in *Scheme 4.6*. However, the cell is expected to deteriorate by acid leaching as the pH goes lower (pH<1), which results in a lower efficiency [8].

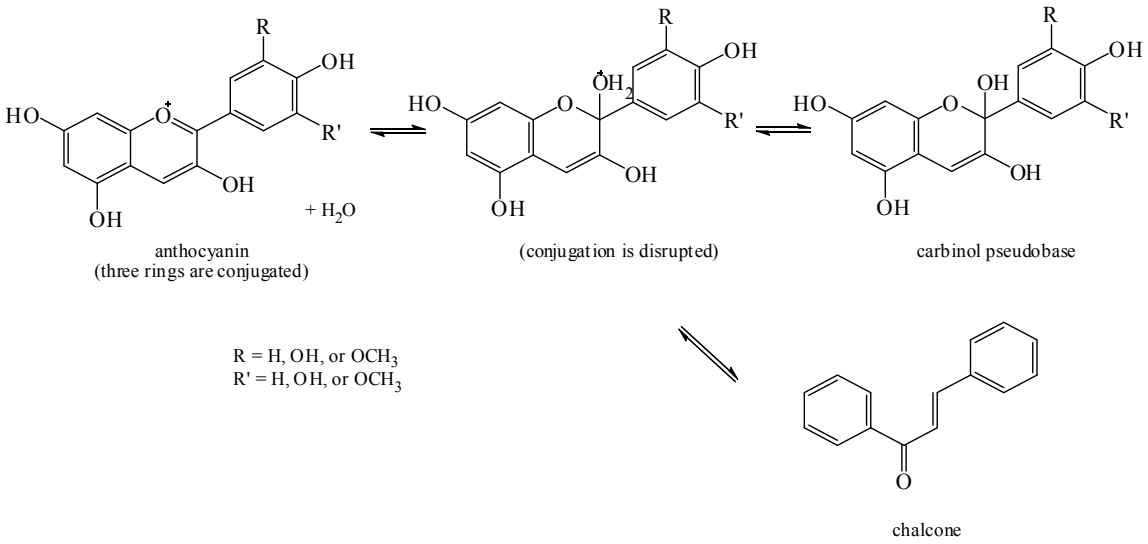

Scheme 4.6: Anthocyanin molecule at different conditions

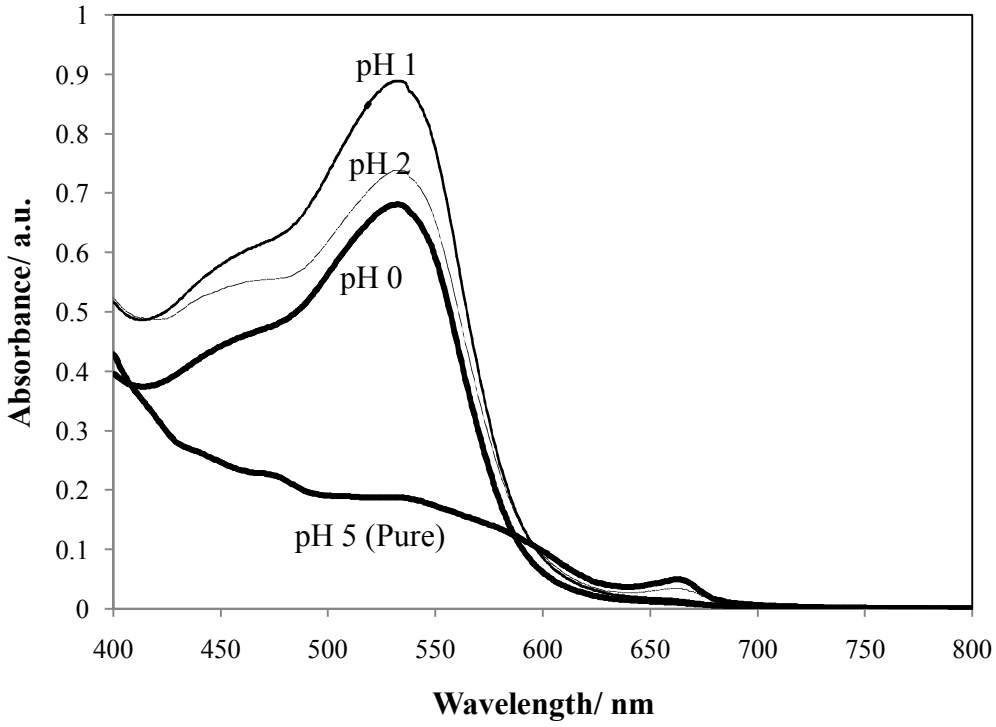

Figure 4.34: UV spectra of dye extracted from black rice

Comparison of UV spectra of dye from black rice extracted from ethanol and TiO_2 layer has been done by S. Hao et al. [80]. Absorption peak wavelength of the dye extracted on TiO_2 layer is shifted to the shorter wavelength compared to that in ethanol solution. The blue shift phenomenon might be caused by three factors:

i. Solvent: the polar solvent, such as in ethanol will result in the red shift of absorption peak wavelength.
ii. Aggregation state: on the surface of TiO_2 film, anthocyanin molecules will array in face to face mode, which leads to the blue shift of absorption peak wavelength.
iii. Functional groups: the anthocyanin molecules absorb on the surface of TiO_2, TiO_2 can be regarded as an electron attracting group which will result in the blue shift of absorption peak wavelength.

4.3.2. Performance of DSSC Using Dye From Red Cabbage

Figure 4.35 depicts the current-voltage characteristics of the DSSCs using dye extracted from red cabbage. From the figure along with *Table 4.10*, it can be seen that pH 1 shows the highest value of fill factor of 0.40. The V_{OC} is 0.28 V and the J_{SC} is 0.32 mA cm^{-2}. However pH 2 shows the highest energy conversion of 0.05 % with a largest value of J_{SC} among all pHs, 0.68 mA cm^{-2}. The V_{OC} and fill factor are 0.27 V and 0.25, respectively. Pure dye solution extracted from red cabbage with pH 5 shows the smallest area under the curve with the lowest J_{SC} of 0.03 mA cm^{-2}.

Since dyes extracted from black rice and red cabbage consist of anthocyanin, it can be seen that the most efficient DSSCs using both dyes performed at pH below 2. As

mentioned previously, pH below 2, anthocyanin exists as flavylium ion, the stable form of anthocyanin and increasing the pH will hydrate this ion to quinonoidal base which is labile. However, at pH lower than 1, the cell might be deteriorated by acid leaching and this explains the lowest value of energy conversion efficiency of pH 0.5 (*Table 4.10)*.

Table 4.10: Performance of DSSCs using dye extracted from red cabbage with different pH

pH of dye	V_{OC} / V	I_{SC}/ mA	J_{SC}/ mA cm^{-2}	FF	*H*
0.5	0.25	0.04	0.16	0.23	0.01
1.0	0.28	0.08	0.32	0.40	0.03
2.0	0.27	0.17	0.68	0.25	0.05
5.0	0.28	0.06	0.03	0.22	0.02

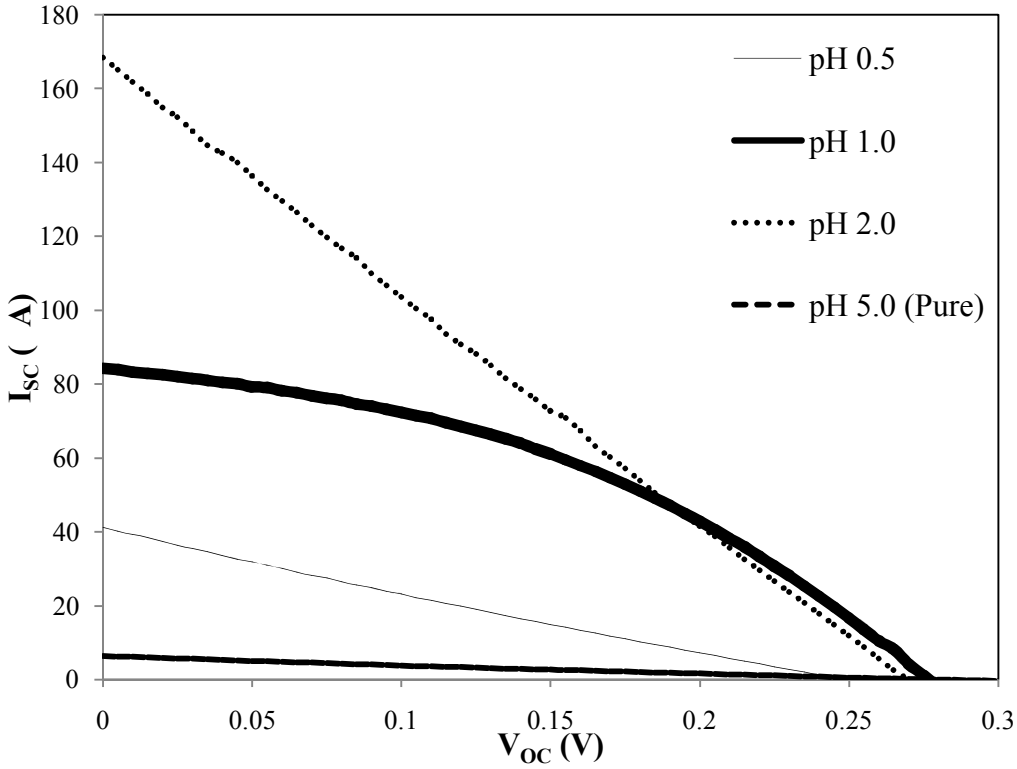

Figure 4.35: Current-voltage curves of DSSC using extracted dye from red cabbage

Figure 4.36 shows the absorption spectra of untreated and acid-treated extracts from red cabbage. The absorption spectrum of the red cabbage having natural pH 5 shows maximum absorption value at 536 nm wavelength with the lowest value of absorption at 0.34 a.u. The curves pattern shows that pH 1 and pH 2 of dyes extracted from red cabbage absorb similar amount of light at wavelength 5.26 nm with highest peak absorption parallel to the greater energy conversion efficiency shown in *Table 4.10*.

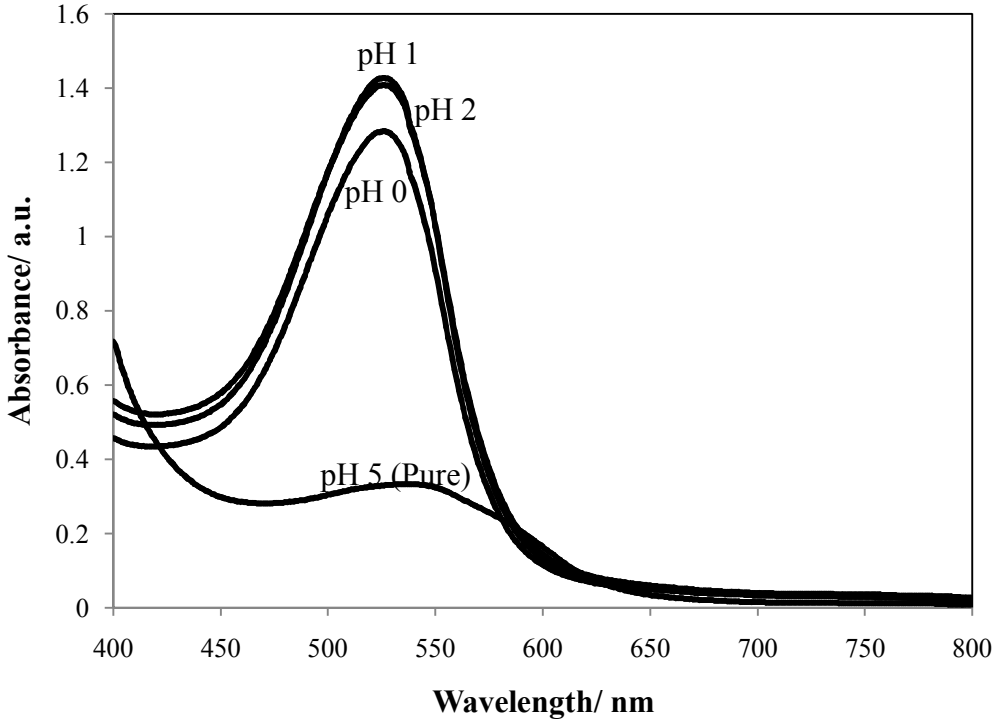

Figure 4.36: UV spectra of dyes extracted from red cabbage

4.3.3. Black rice vs. red cabbage

pHs of the two dyes were compared at pH 1 following the work of Buraidah et. al [118]. Extracted dyes from black rice give a wide area curve compared to the extracted dye

from red cabbage as shown in *Figure 4.37*. The comparison of DSSC parameters such as I_{SC}, V_{OC} and fill factor shown that extracted dye from black rice exhibits the most effective DSSC with the fill factor value of 0.43, V_{OC} of 0.28 V and J_{SC} of 1.24 mA cm^{-2} with 0.25 cm^2 active area. From these results, black rice extracts give better photosensitized effect possibly due to the better interaction between the carbonyl and hydroxyl groups of anthocyanin molecule on black rice extract and the TiO_2 layer on cathode in DSSC.

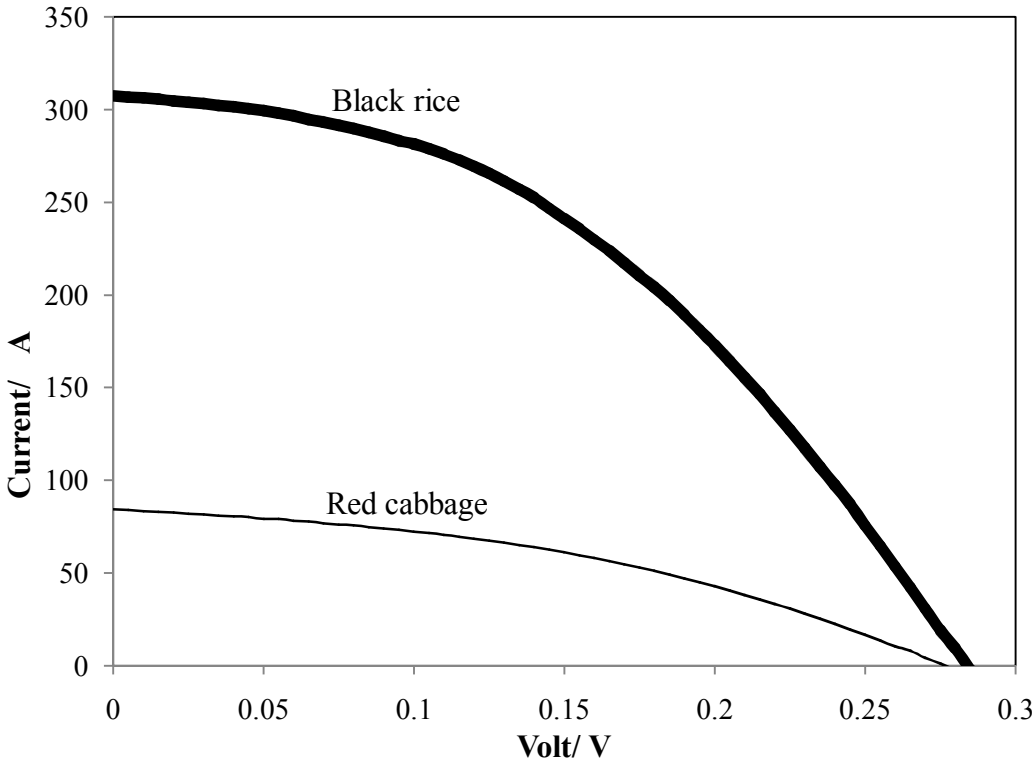

Figure 4.37: I-V curves of DSSC using extracted dyes from black rice and red cabbage at pH 1

The absorption spectra of the acid-treated dye extracts from black rice and red cabbage at pH 1 are shown in *Figure 4.38*. The maximum absorption peak of black rice is at the shorter wavelength of 532 nm compared to the absorption spectrum of the red cabbage

which is at 526 nm. In contrast, the absorbance value of dye from red cabbage (1.43 a.u.) is higher than black rice (0.89 a.u.).

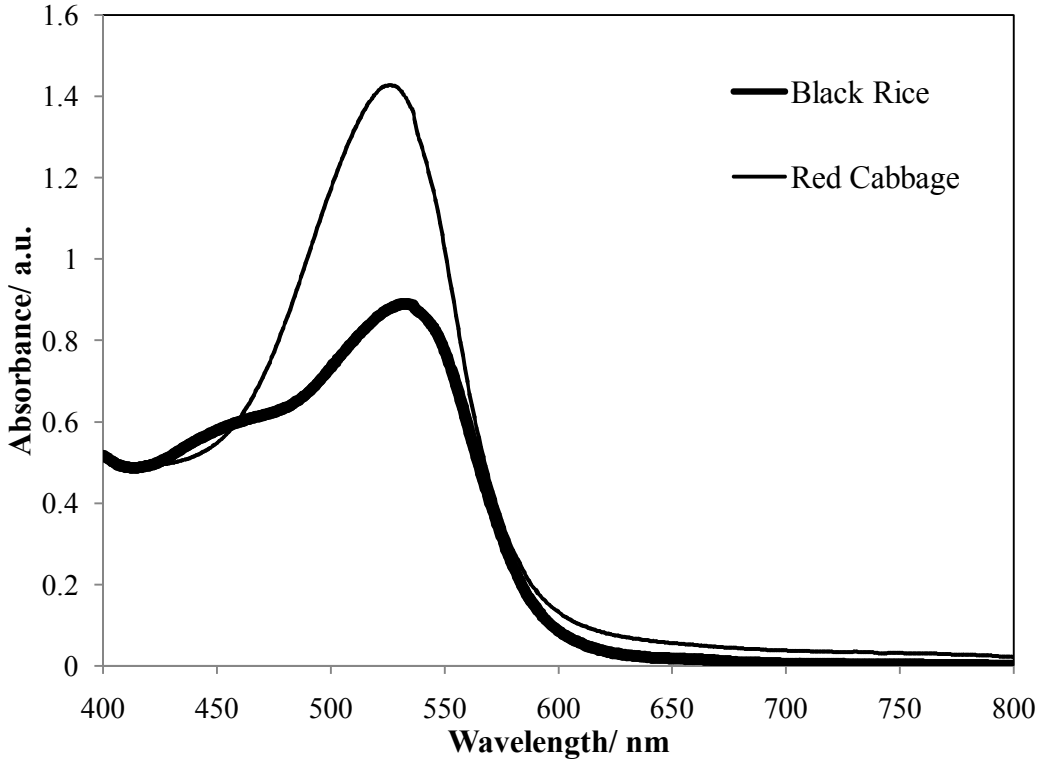

Figure 4.38: UV spectra of dye extracted from black rice and red cabbage.

The difference in the absorption characteristic is due to the different type of anthocyanins and colors of the extracts [8]. The difference in colors of the dye has been mentioned previously in the beginning of *Section 4.3*, that the color of the dye extracted from black rice is purplish-red and from red cabbage is reddish-maroon. *Figure 4.39* shows the chemical structure of anthocyanin mainly present in red cabbage. However, anthocyanin extracted black rice was identified as containing cyaniding-3-glucoside and peonidin-3-glucoside [119] and the chemical structures are shown in *Figure 4.40*.

It can be seen that structure of anthocyanin in red cabbage extract has longer group attached at middle heterocyclic ring, compared to that of cyaniding-3-glucose and peonidin-

3-glucose complexes in black rice extract. This results in a stronger steric hindrance for anthocyanin to form bond with the oxide surface and prevents the anthocyanin molecules from arraying on the TiO_2 layer effectively [80], leading to a deficiency of electron transfer from dye molecule to conducting band of TiO_2.

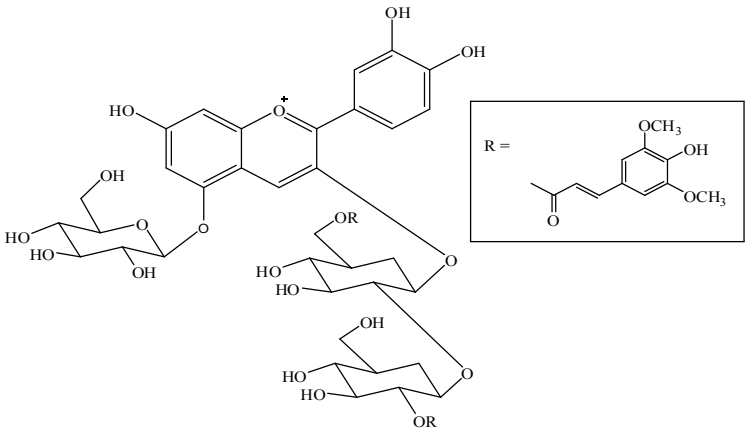

Figure 4.39: Chemical structure of dye mainly present in red cabbage [92]

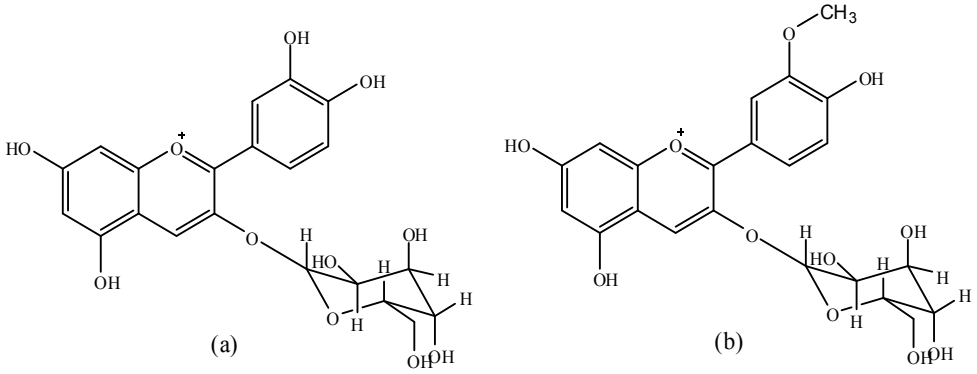

Figure 4.40: Chemical structure of (a) cyaniding-3-glucoside and (b) peonidin-3-glucoside

In conclusion, dye from black rice extract has higher photosensitized performance as compared to the red cabbage due to the differences in the structure of dyes.